HHS Public Access

Author manuscript

Radiat Res. Author manuscript; available in PMC 2021 July 06.

Published in final edited form as:

Radiat Res. 2021 June 01; 195(6): 522–540. doi:10.1667/RADE-20-00237.1.

Low-Dose Radiation Potentiates the Propagation of Anti-Tumor Immunity against Melanoma Tumor in the Brain after *In Situ* Vaccination at a Tumor outside the Brain

Paul A. Clark[a], **Raghava N. Sriramaneni**[a], **Amber M. Bates**[a], **Won Jong Jin**[a], **Justin C. Jagodinsky**[a], **Reinier Hernandez**[b], **Trang Le**[e], **Justin J. Jeffery**[c], **Ian R. Marsh**[b], **Joseph J. Grudzinski**[c], **Eduardo Aluicio-Sarduy**[b], **Todd E. Barnhart**[b], **Bryce R. Anderson**[a], **Ishan Chakravarty**[a], **Ian S. Arthur**[a], **KyungMann Kim**[e], **Jonathan W. Engle**[b,c], **Bryan P. Bednarz**[b], **Jamey P. Weichert**[c], **Zachary S. Morris**[a,d,1]

[a]Department of Human Oncology, University of Wisconsin School of Medicine and Public Health, Madison, Wisconsin

[b]Department of Medical Physics, University of Wisconsin School of Medicine and Public Health, Madison, Wisconsin

[c]Department of Radiology University of Wisconsin School of Medicine and Public Health, Madison, Wisconsin

[d]Department of Carbone Cancer Center, University of Wisconsin School of Medicine and Public Health, Madison, Wisconsin

[e]Department of Biostatistics and Medical Informatics, University of Wisconsin-Madison, Madison, Wisconsin

Abstract

Brain metastases develop in over 60% of advanced melanoma patients and negatively impact quality of life and prognosis. In a murine melanoma model, we previously showed that an *in situ* vaccination (ISV) regimen, combining radiation treatment and intratumoral (IT) injection of immunocytokine (IC: anti-GD2 antibody fused to IL2), along with the immune checkpoint inhibitor + anti-CTLA-4, robustly eliminates peripheral flank tumors but only has modest effects on co-occurring intracranial tumors. In this study, we investigated the ability of low-dose radiation to the brain to potentiate anti-tumor immunity against a brain tumor when combined with ISV + anti-CTLA-4. B78 ($GD2^+$, immunologically "cold") melanoma tumor cells were implanted into the flank and the right striatum of the brain in C57BL/6 mice. Flank tumors (50–150 mm^3) were treated following a previously optimized ISV regimen [radiation (12 Gy × 1, treatment day 1), IT-IC (50 lg daily, treatment days 6–10), and + anti-CTLA-4 (100 lg, treatment days 3, 6, 9)]. Mice that additionally received whole-brain radiation treatment (WBRT, 4 Gy × 1) on day 15 demonstrated significantly increased survival compared to animals that received ISV + anti-CTLA-4 alone, WBRT alone or no treatment (control) ($P < 0.001$, log-rank test). Timing of WBRT was critical, as WBRT administration on day 1 did not significantly enhance survival compared to

[1]Address for correspondence: WIMR-I Building, Room 3131, 1111 Highland Ave., Madison, WI 53705; zmorris@humonc.wisc.edu.

ISV + anti-CTLA-4, suggesting that the effect of WBRT on survival might be mediated through immune modulation and not just direct tumor cell cytotoxicity. Modest increases in T cells ($CD8^+$ and $CD4^+$) and monocytes/macrophages ($F4/80^+$) but no changes in $FOXP3^+$ regulatory T cells (Tregs), were observed in brain melanoma tumors with addition of WBRT (on day 15) to ISV + anti-CTLA-4. Cytokine multiplex immunoassay revealed distinct changes in both intracranial melanoma and contralateral normal brain with addition of WBRT (day 15) to ISV + anti-CTLA-4, with notable significant changes in pro-inflammatory (e.g., IFNγ, TNFα and LIX/CXCL5) and suppressive (e.g., IL10, IL13) cytokines as well as chemokines (e.g., IP-10/CXCL10 and MIG/CXCL9). We tested the ability of the alkylphosphocholine analog, NM600, to deliver immunomodulatory radiation to melanoma brain tumors as a targeted radionuclide therapy (TRT). Yttrium-86 (^{86}Y) chelated to NM600 was delivered intravenously by tail vein to mice harboring flank and brain melanoma tumors, and PET imaging demonstrated specific accumulation up to 72 h at each tumor site (~12:1 brain tumor/brain and ~8:1 flank tumor/muscle). When NM600 was chelated to therapeutic β-particle-emitting ^{90}Y and administered on treatment day 13, T-cell infiltration and cytokine profiles were altered in melanoma brain tumor, like that observed for WBRT. Overall, our results demonstrate that addition of low-dose radiation, timed appropriately with ISV administration to tumors outside the brain, significantly increases survival in animals co-harboring melanoma brain tumors. This observation has potentially important translational implications as a treatment strategy for increasing the response of tumors in the brain to systemically administered immunotherapies.

INTRODUCTION

In situ tumor vaccination (ISV) is a cancer treatment strategy with the aim of converting a patient's own tumor into a nidus for presentation of tumor antigens to activate and expand an anti-tumor T-cell response (1). Preclinical and clinical studies have demonstrated that hypofractionated, moderate-dose external beam radiation treatment targeting a single tumor site can elicit an ISV effect and thereby improve the anti-tumor immune response to immune checkpoint inhibitors such as anti-PD-1 or anti-CTLA-4 (2–8). This reflects the capability of moderate-dose radiation to enhance tumor antigen presentation, resulting in greater diversity of antigen recognition by the anti-tumor T-cell response (7, 8). While clinical studies indicate safety for combinations of external beam radiation therapy and immune checkpoint inhibitors (9), they have not yet conclusively demonstrated that focal radiation alone can enhance the systemic anti-tumor response to checkpoint blockade (10, 11).

We previously reported that the ISV effect of radiation therapy can be augmented in preclinical studies by combination with local injection of tumor-specific antibody and the immune-stimulatory cytokine IL2 (12, 13). This combined-modality ISV regimen rendered immunologically "cold" tumors responsive to immune checkpoint blockade; and, when combined with anti-CTLA-4 therapy, this regimen resulted in much more effective tumor clearance and activation of tumor-specific immune memory than radiation alone (12). We are now evaluating this treatment approach in patients with metastatic melanoma in a phase I/II trial (NCT03958383). Although this ISV regimen consistently results in a potent systemic anti-tumor immune response in mice leading to complete response at distant tumor sites that are not directly treated with radiation or intratumoral injection (12), we recently

reported that this treatment is much less effective in controlling tumor that is present in the brain at time of treatment (13). This is consistent with prior studies demonstrating the restrictive effects of the brain tumor microenvironment on anti-tumor immunity (14–19).

Brain metastases commonly develop in patients with advanced cancers and frequently carry a poor prognosis along with detrimental effects on quality of life (20). Some cancers such as melanoma have a strong proclivity for spread to the brain. Immune checkpoint inhibition with anti-PD-1 and/or anti-CTLA-4 is standardly used to treat patients with metastatic melanoma (21). Recently published studies demonstrate that, in approximately one half of patients with small, asymptomatic melanoma brain metastases, immune checkpoint blockade can elicit a response (22–24). The remainder of patients with larger, symptomatic or non-responsive melanoma brain metastases typically require brain-directed treatment including surgical resection and/or high-dose radiotherapy. When individual tumor sites cannot be targeted with focal therapy due to excessive burden of disease, then whole-brain radiation therapy (WBRT) is commonly employed (25). Unfortunately, in the latter circumstance, the dose of radiation provided is often too low to confer durable or complete control of brain metastases and yet high enough to confer considerable risk for neurocognitive toxicities that negatively affect patient quality of life (25).

While moderate- to high-dose (8–12 Gy/fraction) hypofractionated radiation may be optimal for priming an ISV effect (26), we have been investigating the potential capability of low-to-moderate-dose radiation (2–4 Gy) to enhance the propagation of such an effect. Although ISV may prime a more effective T-cell response, when these effector T cells circulate to nonirradiated tumors, particularly those in immune-restrictive locations like the brain, they encounter a suppressive tumor microenvironment and poorly susceptible tumor cells (13, 27). In mice with multiple extracranial tumors, we recently observed that delivery of radiation to the secondary melanoma tumor sites enhances the efficacy of ISV or ISV + anti-CTLA-4 directed at a single tumor site (27). Prior preclinical studies from other groups have demonstrated that 4 Gy WBRT can enhance the response of a primary glioma brain tumor model to a peripheral *in situ* vaccination (28). Based on those observations, we hypothesize that low-to-moderate-dose radiation could be safely delivered to metastatic tumor sites in the brain using WBRT or targeted radionuclide therapy and that in doing so we might render these sites more permissive to the propagation of anti-tumor immunity from an ISV.

MATERIALS AND METHODS

Cell Lines

B78-D14 (B78) melanoma was derived from B16 melanoma, as described elsewhere (29) and was obtained from Ralph Reisfeld (Scripps Research Institute, La Jolla, CA) in 2002. All cancer cells were cultured in RPMI-1640 medium supplemented with 10% FBS, 2 mmol/l L-glutamine, 100 U/ml penicillin and 100 μg/ml streptomycin, as described elsewhere (12). Cell authentication was performed per ATCC guidelines using morphology, growth curves, and mycoplasma testing within 6 months of use and routinely thereafter.

Murine Tumor Models

All animal studies were approved by the Institutional Animal Care and Use Committee (IACUC) at the University of Wisconsin-Madison (Madison, WI). Female mice (C57BL/6) were purchased at 6-to-8 weeks of age from Taconic Biosciences, Inc. (East Greenbush, NY) and used for all experiments. Mouse experiments were repeated in two or more independent trials with at least 4 animals per treatment group in each trial; aggregate number of animals (n) is indicated. C57BL/6-Tg (Foxp3 DTR/EGFP) 23.2 Spar/Mmjax "DEREG" mice were purchased from the Jackson Laboratory (MMRRC; Bar Harbor, ME). Treg depletion with diphtheria toxin was achieved following a prior methodology, as reported elsewhere (13, 27, 30) by daily intraperitoneal (i.p.) injection of 1 μg diphtheria toxin (MilliporeSigma, St. Louis, MO) diluted in PBS for 2 days at day 14 and 15 postirradiation, to ensure presence of melanoma brain tumor prior to Treg depletion. We have previously demonstrated Treg depletion >40% knockdown by day 3 (1 day after completion of two DT injections of 1 μg) (13), with previously reported studies indicating >90% depletion by day 7 (31). At euthanasia, mice were dissected and grossly examined for brain tumor to verify no confounding effect of Treg depletion on autoimmunity and subsequent mortality (31).

Therapeutic Agents

hu14.18-IL2 was provided by Apeiron Biologics (Vienna, Austria) (32). The hu14.18 antibody component of this immunocytokine (IC) targets GD2, which is expressed in many human melanomas (33). The B78 melanoma line is derived from B16 melanoma and engineered to express GD2 (29). anti-CTLA-4 (clone 9D9) was provided by Bristol Myers Squibbe (New York, NY). For targeted radionuclide therapy (TRT), the positron emitter ^{86}Y was produced as described elsewhere (34, 35). Briefly, ^{86}Y was produced in a PETrace cyclotron (GE Healthcare, Chicago, IL) via proton (15.2 MeV) bombardment of enriched [^{86}Sr]$SrCO_3$ (96.4 ± 0.1%) solid targets. Irradiated targets were dissolved in 6 N hydrochloric acid (HCl) and ^{86}Y was isolated from solution with DGA extraction resin in ~600 μl of 0.1 *M* HCl. Clinical-grade $^{90}YCl_3$ was purchased from PerkinElmer®, Inc. (Waltham, MA) and 2-(trimethylammonio)ethyl(18-(4-(2-(4,7,10-tris(carboxymethyl)-1,4,7,10-tetraazacyclododecan-1-yl)acetamido)-phenyl)octadecyl) phosphate (NM600) was kindly provided by Archeus Technologies (Madison, WI).

External Beam Irradiation

External beam irradiation was delivered to *in vivo* tumors using an X-RAD 320 (Precision X-Ray Inc., North Branford, CT), as described elsewhere (12, 13). Mice were immobilized using custom lead jigs that exposed the dorsal right flank, or the whole head for WBRT. For the *in vivo* ISV + anti-CTLA-4 regimen, flank tumors received a single dose of 12 Gy. For WBRT, mice were briefly anesthetized with isoflurane prior to immobilization in the lead jig and delivery of a single 4 Gy dose of radiation to the whole head.

In Situ Vaccination

An ISV + anti-CTLA-4 regimen previously reported by our group was used to treat melanoma in the flank (Fig. 1A). This immunotherapeutic regimen induces long-term regression of flank melanomas (12, 27), but only minimal survival benefit for mice co-

harboring intracranial melanoma metastases (13). Briefly, B78 ($GD2^+$) "primary" tumors were engrafted by intradermal right flank injection of 2×10^6 cells. Tumor size was determined using calipers and volume approximated as ($width^2$ × length)/2. Mice were randomized immediately prior to treatment. Treatment began when primary tumors were well established (50–150 mm^3 tumor volume). Radiation (12 Gy, single fraction) administration was defined as "day 1" of treatment. Intratumoral (IT) IC injections were performed by a single percutaneous needle puncture followed by injection of 50 μg of hu14.18-IL2 in 100 μl volume with needle redirection to distribute injected material around the tumor. IT-IC was administered daily on treatment days 6–10. Together, radiation + IT-IC constitute the ISV approach. Finally, the + anti-CTLA-4 antibody was administered by 100 μg i.p. injections on treatment days 3, 6 and 9.

Low-dose WBRT (4 Gy, single fraction) was administered on either day 1 immediately after flank irradiation or day 15 to examine timing differences. We have previously demonstrated day 15 as approximately peak T-cell response time for our ISV regimen (12, 27).

Mice were monitored for survival and euthanized upon signs of neurological impairment, moribund status or humane end points as per IACUC guidelines. At euthanasia, mice were dissected and grossly examined to verify brain tumor. Therapeutic "complete response" was defined as mice having no remaining visible tumor or neurological symptoms at treatment day 60. We have previously demonstrated that this memory response is T-cell dependent (12, 13).

Orthotopic Brain Injection

Intracranial implantation of cancer cells was performed as described elsewhere (13, 36). Briefly, B78 (2×10^5 cells) were injected intracranially ~24 h prior to irradiation of a pre-existing flank tumor at coordinates referenced from bregma: 0 mm antero-posterior, +2.5 mm medio-lateral and −3.5 mm dorso-ventral. At specific time points or at onset of neurological symptoms, tumor-bearing mice were euthanized, and brains excised, grossly examined for presence of tumor and processed for further analyses.

Radiochemistry for NM600

As described elsewhere (37), NM600 was radiolabeled with $^{86}YCl_3$ as no-carrier-added formulation to obtain [^{86}Y]Y-DOTA-NM600 (hereafter simplified to ^{86}Y-NM600) for positron emission tomography (PET) imaging and dosimetry; for therapeutic treatments, NM600 was radiolabeled with $^{90}YCl_3$ to obtain ^{90}Y-DOTA-NM600 (hereafter simplified to ^{90}Y-NM600). Radiolabeling of NM600 with $^{86/90}$Y was performed by mixing 185–370 MBq (5 −10 mCi) of $^{86/90}$Y and 54–81nmol/GBq (10–15 nmol/mCi) of NM600 in 0.1 *M* NaOAc (pH = 5.5) buffer. After incubation at 90°C for 30 min under constant shaking (500 rpm), $^{86/90}$Y-NM600 was purified by solid phase extraction using an HLB cartridge (Waters™ Corp., Milford, MA). For *in vivo* use, $^{86/90}$Y-NM600 was formulated in vehicle consisting of normal saline containing 0.4% v/v Tween™ 20 and sodium ascorbate (0.5% w/v). Yields and radiochemical purity were consistently >95%, and a similar apparent molar activity of 18 GBq/μmol was obtained for both ^{86}Y-NM600 and ^{90}Y-NM600. Additionally, radiotracer

stability *in vivo* has been demonstrated from mouse serum samples up to 48 h, with no significant radio peaks corresponding to metabolites observed (37).

Targeted Radionuclide Therapy (TRT) Imaging and Dosimetry

B78 cells were injected into the mouse brain (2×10^5) and flank (2×10^6) and allowed to grow for 18 days (13). B78 brain tumor growth was then verified with magnetic resonance imaging (MRI) using T1-weighted images with gadolinium enhancement, as described elsewhere (36). Longitudinal PET scanning was then performed to quantify ^{86}Y-NM600 tumor uptake and biodistribution and estimate tumor dosimetry of ^{90}Y-NM600, as described elsewhere (37). Mice bearing MRI-verified B78 intracranial and flank tumors (n = 4) were injected intravenously (i.v., lateral tail vein) with 11.77–12.03 MBq of ^{86}Y-NM600 and sequential CT (80 kVp; 1,000 mAs; 220 angles) and static PET scans consisting of 80 million coincidence events (time window: 3.432 ns; energy window: 350–650 keV) were acquired in an Inveon microPET/microCT scanner (Siemens Medical Solutions, Knoxville, TN) at 2, 24, 48 and 72 h after injection of the radiotracer. Prior to each scan, pairs of mice were anesthetized with isoflurane (4% induction; 2% maintenance) and placed on the scanner bed in the prone position. List-mode PET scans were reconstructed using a three-dimensional (3D) ordered subset expectation maximization/maximum posteriori (OSEM3D/MAP) algorithm (MAP subsets: 16, MAP iterations: 18; OSEM3D iterations in MAP reconstruction: 2, without scatter), and the resulting images were fused with the CT images for attenuation correction and anatomical referencing. Region-of-interest (ROI) analysis of the PET images was performed to determine the magnitude and kinetics of ^{86}Y-NM600 uptake in the tumor and normal tissues of interest. Quantitative data were expressed as percentage injected dose per gram of tissue (%ID/g; mean ± SE). *Ex vivo* biodistribution was performed after the final imaging time point at 72 h after injection of ^{86}Y-NM600 to corroborate the accuracy of the image-derived quantification. After PET/CT scan, mice were sacrificed by CO_2 asphyxiation, B78 tumors (flank and brain) and several normal tissues were collected, wet-weighed, counted in an automated gamma-counter (Wizard^{2TM}, PerkinElmer), and the %ID/g (mean ± SE) corresponding to each tissue was calculated.

A Monte Carlo-based dosimetry assessment platform, RAPID, was used to estimate pre-clinical dose distributions in mouse-specific anatomy (35, 38, 39). CT and the PET images were used in the Monte Carlo simulation to define the geometry and the source distribution, respectively. Each PET volume was imported into the Monte Carlo framework (Geant4 version 9.6) and used to define source terms in the simulation. To generate the simulation geometry, CT volume data consisting of Hounsfield units (HU) were transformed into mass densities by applying the HU-to-density CT scanner-specific calibration curve. Using libraries from the Evaluated Nuclear Structure Data File (ENDSF) database (Brookhaven National Laboratory, Upton, NY), which includes all beta and gamma radiation emitted per decay, each source decay was sampled uniformly throughout each voxel and the energy deposition was tracked to create 3D dose-rate distributions. Cumulative absorbed dose was then calculated by integrating the mean dose rate in each ROI.

CT-based contours of the tumor and normal organs of interest were used to quantify the *in vivo* concentration of NM600 over time (pharmacokinetics) and describe the spatial

distribution of the absorbed dose imparted by ^{90}Y-NM600 (dosimetry). This subject-specific dosimetry platform has been implemented clinically as well to estimate the dosimetry of radio-iodinated APCs (40–42).

A novel segmentation methodology was performed to estimate dosimetry in the brain tumor. First, thresholding of the T1-weighted, gadolinium enhancement MRI images was used to delineate the brain tumor. Next, a region-specific rigid image registration algorithm was performed to align the MRI and CT images of the mouse brain. Then, the MRI-based brain tumor contour was propagated onto the CT image volume to create a CT contour.

TRT Therapeutic Analyses

For ^{90}Y-NM600 therapeutic studies, mice were injected with B78 melanoma cells in the flank and allowed to grow tumors as for the ISV + anti-CTLA-4 regimen. B78 melanoma cells (200,000) were injected intracranially on day −8. Day 1 was defined as start of ISV + anti-CTLA-4 regimen, and ^{90}Y-NM600 was administered on day 13. Taken together, 90Y-NM600 was administered 21 days after B78 cell intracranial injection. This timing was selected so that ^{90}Y-NM600 delivery would be made at a time when melanoma brain tumor burden matched that from dosimetry studies performed with ^{86}Y-NM600 imaging. A single dose of 3.7 MBq was i.v. injected via tail vein. The timing of ISV + anti-CTLA-4 administration for cohorts receiving that regimen was kept constant with other experiments and delivered between treatment days 1–10. Mice were then monitored for survival as described above. Upon survival end point of moribund status due to tumor burden, mice were euthanized, and brains excised, grossly examined for presence of tumor, and fixed in 10% formalin. The radioisotope within the tissue was allowed time to reduce to background (10 half-lives), at which time brains were processed for further analyses.

Immunohistochemistry

Immunohistochemistry (IHC) was performed on formalin-fixed paraffin-embedded (FFPE) samples. Antibodies used were: CD4 (mAb Rat IgG1, kappa; clone 4SM95; eBioscience™ Inc., San Diego, CA, 1:500), CD8a (mAb Rat IgG2a, lambda; clone 4SM15; eBioscience, 1:250), FOXP3 (mAb Rat IgG2a, kappa; clone FJK-16S; eBioscience, 1:500), F4/80 (mAb Rabbit IgG; clone D2S9R; Cell Signaling Technology® Inc., Danvers, MA, 1:200). Standard IHC methods were performed as described elsewhere (12, 43). All labeling was performed with no primary antibody negative controls. A minimum of three random high-power fields per tumor sample were quantified for positive labeling by a blinded observer, with serial slides of H&E used to determine viable tumor areas. For F4/80 immunolabeling, individual labeled cells were difficult to distinguish and therefore, percentage labeled area was calculated using multiple color-balanced 20× fields and ImageJ “Color Deconvolution (H DAB)” (National Institutes of Health, Bethesda, MD), followed by thresholding of the deconvoluted DAB image (13). The multiple high-power fields were averaged for each individual tumor sample (i.e., mouse) to achieve a single “n” for statistical purposes; results were charted as mean ± SE with data points representing individual mice (“n”).

Flow Cytometry

Flow cytometry was used to analyze immune cell populations (12, 13, 44) in a minimum of three samples in two independent animal studies. Dissected intracranial melanoma tumors were physically dissociated and filtered through a 70-μm cell filter. Single cells were labeled with primary antibody. Cells without primary antibody labeling were used as unlabeled negative controls; fluorescent beads (UltraComp eBeads™, Invitrogen™, Carlsbad, CA) were used as positive/calibration controls and to determine compensation between fluorescent channels. Forward- and side-scatter gating identified single cells and viable cell (Ghost Dye™ Red 780 Viability Dye, 1:100; Tonbo Biosciences, San Diego, CA) exclusion identified live cells. Fluorescence minus one (FMO) methodology was used to determine gating. Flow cytometry was performed on an Attune NxT Flow Cytometer (Thermo Fisher Scientific™ Inc., Waltham, MA), and compensation matrix computed and data analyzed using FlowJo version 9 software (Ashland, OR) following published flow cytometry guidelines (45).

Antibodies used were: CD4 (BV510, 1:400, clone RM4–5), CD8 (PerCP-cy5.5, 1:200, clone 53–6.7), FOXP3 (BV421, 1:100, clone MF-14), all acquired from BioLegend® Inc. (San Diego, CA); and CD45 (PE-cy7, 1:200, clone 30-F11), CD3 (FITC, 1:200, clone 17A2), both acquired from Tonbo Biosciences.

qRT-PCR

For analysis of tumor tissue, tumor samples were homogenized using a Bead Mill Homogenizer (Bead Ruptor Elite; Omni International, Kennesaw, GA). Total RNA was extracted after sample homogenization using RNeasy Mini Kit (QIAGEN®, Valencia, CA) according to the manufacturer's instructions. Extracted RNA was subjected to complementary cDNA synthesis using QuantiTect Reverse Transcription Kit (QIAGEN) according to the manufacturer's instructions. TaqMan® probes and TaqMan Fast Advanced Master Mix were purchased from Thermo Fisher Scientific and quantitative reverse transcription polymerase chain reaction (qRT-PCR) performed according to manufacturer protocol. The reaction (5 μl total volume) was prepared using Labcyte Echo® 550 and Formulatrix® TEMPEST® liquid handling systems. Thermal cycling conditions (QuantStudio™ 6, Applied Biosystems®, Carlsbad, CA) included the UNG incubation stage at 50°C for 2 min, followed by polymerase activation stage at 95°C for 2 min followed by 40 cycles of each PCR step: (denaturation) 95°C for 1 s and (annealing/extension) 60°C for 20 s. For data analysis, the Ct values were exported to an Excel file and fold-change was calculated using the DDCt method. *Hprt* was used as endogenous control. The following TaqMan probes were used: *Mx1* (Mm00487796_m1), *Ifnb1* (Mm00439552_s1), *Mhc-1/H2-k1/H2-d1* (Mm04208017_mH), *Pd-l1/Cd274* (Mm03048248_m1), *Nos2* (Mm00440502_m1) and *Arg1* (Mm00475988_m1).

Tumor Cytokine Multiplex Immunoassay

Tumor weight was recorded and 5 μl/mg of Cell Lysis Buffer with PMSF (Cell Signaling Technology) and Halt™ Phosphatase Inhibitor Cocktail (Thermo Fisher Scientific) were added to the tumor. Tumors were homogenized in bead beater tubes, and the lysates were stored at −80°C until use. A multiplex immunoassay was used to determine the

concentration of 32 cytokines and chemokines in the tumor lysates (MILLIPLEX® MAP Mouse Cytokine/Chemokine Magnetic Bead Panel, MilliporeSigma) following the manufacturer's instructions. The multiplex was read on the MAGPIX System (MilliporeSigma), and the protein concentrations were interpolated from curves constructed from the protein standards and their respective median fluorescence intensity (MFI) readings (MILLIPLEX Analyst, MilliporeSigma). Log and Z-transformation of the data was performed using SPSS® (IBM® Corp., Armonk, NY) and followed by unbiased hierarchical clustering (clustering only cytokines or both animals and cytokines) using an on-line tool [Next Generation Clustered Heat Maps (NG-CHM), MD Anderson Cancer Center, University of Texas (Houston, TX), http://www.ngchm.net/; Euclidean distance metric and Ward agglomeration] (46). The same experimental group, ISV + anti-CTLA-4, was used for both multiplex immunoassay experiments.

Statistical Analyses

All results are displayed as mean ± standard error (SE) of the mean, unless otherwise noted. Survival curves were estimated using the Kaplan-Meier method; a log-rank pairwise comparison test with Benjamini-Hochberg adjustment for P values was used to assess multiple comparisons of overall survival between treatment groups. For the WBRT survival experiment, a Cox proportional hazards regression model was fitted with ISV (0-no-ISV and 1-yes-ISV), WBRT (non-WBRT, WBRT-D1, WBRT-D15) and their interactions as fixed effects. Time was calculated from date of treatment until death. Mice that were alive at a predetermined time point were censored. Student's t test was used for two-sample comparisons in TRT experiment comparing brain versus flank tumor/normal tissue ratios. Two-way ANOVA and Bonferroni's method for P value adjustments were used for 2× 2 factorial designs to assess the multiple comparison among groups. $P < 0.05$ was considered significant and is indicated in the figures as: $^{***}P < 0.001$; $^{**}P < 0.01$; $^{*}P < 0.05$; NS: non-significant ($P \geq 0.05$). Two-sample and multiple comparison analyses were performed using IBM SPSS version 25 or GraphPad Prism version 8 software (La Jolla, CA); Cox regression and survival analyses were performed using R version 4.0.2. All statistical tests were two-sided.

RESULTS

Low-Dose Whole-Brain Irradiation Enhances ISV Effect against Brain Tumor Sites

To begin testing the hypothesis that the anti-tumor efficacy at a brain tumor site could be enhanced by adding low-to-moderate-dose brain radiation to an ISV + anti-CTLA-4 regimen when the ISV, which includes RT + IT-IC, was administered to an extracranial flank tumor, we established a model of melanoma with brain metastases by engrafting "primary" B78 tumors on the right flank and 3–4 weeks later stereotactically injecting B78 tumor cells into the right striatum of the brain to model micro-metastatic tumor. Mice received irradiation (12 Gy, day 1), IC (hu14.18-IL2, 50 μg IT injected daily, days 6–10), and + anti-CTLA-4 (100 μg i.p. injected, days 3, 6 and 9) (12, 13). WBRT was administered as a single 4 Gy fraction either on day 1 immediately after flank irradiation or on day 15 (Fig. 1A). Mice were then monitored for survival. The 4 Gy radiation dose was selected because of its expected safety and feasibility, given that this is a dose routinely delivered as a part of a

standard clinical regimen of WBRT (4 Gy × 5 fractions) (25) and because this single-fraction dose has previously been observed to enhance the propagation of an immune response from a peripheral vaccination against a primary glioma tumor model (28). Non-tumor-bearing mice receiving 4 Gy WBRT did not display significant differences in weight or body condition score (47) up to 28 days, compared to untreated controls, suggesting no acute toxicity of 4 Gy WBRT (Supplementary Fig. S1; https://doi.org/10.1667/RADE-20-00237.1.S1).

Addition of 4 Gy WBRT significantly extended survival of mice receiving ISV + anti-CTLA-4 compared to untreated, WBRT alone or ISV + anti-CTLA-4 only groups ($n \geq 10$, $P < 0.001$; Fig. 1B). A 2-factorial Cox regression additionally confirmed that WBRT at day 15 conferred a significant effect when added to ISV + anti-CTLA-4 (Supplementary Table S1; https://doi.org/10.1667/RADE-20-00237.1.S1). Monitoring of mice after day 60 demonstrated long-term cure of 1 of 10 mice receiving ISV + anti-CTLA-4 + day 15 WBRT, with all other mice eventually dying from brain disease as confirmed by gross dissection at euthanasia. The long-term surviving mouse also did not display any apparent toxicities or gross behavioral changes, suggesting no significant long-term radiation toxicities from 4 Gy WBRT. Importantly, the timing of WBRT administration was critical for efficacy. Administration on day 1 (immediately after flank irradiation) showed no significant increase in survival compared to when WBRT was delivered on day 15. Day 15 of ISV + anti-CTLA-4 regimen approximates T-cell peak response (12, 27). This difference in timing of WBRT efficacy implicates an immunotherapeutic mechanism and not direct tumor cell killing because the latter effect would be expected to be more pronounced at an earlier time point when WBRT was delivered to a considerably lower tumor burden. Notably, 4 Gy WBRT alone delivered either day 1 or day 15 had minimal effect on survival when compared to untreated mice and WBRT alone on day 1 trended towards greater effect compared to WBRT alone on day 15. These observations support our hypothesis and suggest that WBRT on day 15 enhanced response to ISV + anti-CTLA-4 by improving the propagation of anti-tumor immunity to the brain tumor site.

Brain Tumor-Infiltrating Immune Cell Analyses after Addition of WBRT to ISV with + anti-CTLA-4

To begin investigating immunologic mechanisms whereby WBRT might improve survival when added on day 15 to our ISV + anti-CTLA-4 regimen, we analyzed T-cell responses to WBRT with or without ISV + anti-CTLA-4 treatment using immunohistochemistry. We have previously demonstrated a major role for T cells in extracranial as well as intracranial melanoma response to ISV + anti-CTLA-4 (12, 13). Mice were injected with flank and intracranial B78 tumors as above, received ISV + anti-CTLA-4 regimen and WBRT on day 15, and T-cell responses were then analyzed via immunohistochemistry at day 20 (5 days after WBRT) (Fig. 2A). Increased numbers of cytotoxic $CD8^+$ T cells were seen with the addition of WBRT to ISV + anti-CTLA-4 compared to all other groups [$P < 0.05$; $n \geq 9$; mean ± SE CD8: Untreated: 39 ± 5.6 cells per 20× field; WBRT (day 15, 4 Gy): 42 ± 4.8; ISV + anti-CTLA-4: 71 ± 13; WBRT + ISV + anti-CTLA-4: 88 ± 13], but interestingly, no effect was seen on $FOXP3^+$ regulatory T cells (Treg) ($n \geq 9$; mean ± SE FOXP3: Untreated: 51 ± 8.0 cells per 20× field; WBRT (day 15, 4 Gy): 44 ± 6.4; ISV + anti-CTLA-4: 54 ± 6.7;

WBRT ISV + anti-CTLA-4: 48 ± 8.4). Importantly, the ratio of $CD8^+$+:$FOXP3^+$ T cells is a powerful prognostic marker in clinical and preclinical studies of melanoma and other tumor types, corresponding with the strength of adaptive anti-tumor immune response (8, 48–50). We observed a significant increase in the CD8:FOXP3 ratio at the brain tumor site in mice that received WBRT + ISV + anti-CTLA-4 compared to all other treatment groups [$P < 0.05$; n ≥ 9; mean ± SE; CD8/FOXP3 ratio: Untreated: 0.83 ± 0.092; WBRT (day 15, 4 Gy): 1.0 ± 0.11; ISV + anti-CTLA-4: 1.4 ± 0.18; WBRT + ISV + anti-CTLA-4: 1.90 ± 0.10]. The number of $CD4^+$ T cells was also increased with ISV + anti-CTLA-4 compared to untreated and WBRT alone + groups, but remained similar with and without WBRT addition to ISV + anti-CTLA-4 [n ≥ 9; mean ± SE; CD4: Untreated: 51 ± 7.3 cells per 20× field; WBRT (day 15, 4 Gy): 63 ± 9.7; ISV + anti-CTLA-4: 110 6 17; WBRT ISV + anti-CTLA-4: 110 ± 16]. Similar trends of increased $CD8^+$ T cells and CD8:FOXP3 ratio were found using flow cytometry with and without WBRT added to the ISV + anti-CTLA-4 regimen (Supplementary Fig. S2; https://doi.org/10.1667/RADE-20-00237.1.S1).

In previously published studies we demonstrated that Tregs can play a crucial role in limiting the propagation of ISV at extracranial tumor sites and that transient depletion of Tregs after ISV could lead to greater response at both ISV-targeted and distant extracranial melanoma sites (27). Therefore, we tested whether depletion of Tregs would augment response to ISV at a brain melanoma tumor site using the C57BL/6 “DEREG” mouse model in which the diphtheria toxin (DT) receptor is expressed in FOXP3-expressing cells. This model enables depletion of Tregs upon treatment with DT (13, 31). After DT injections on days 1 and 2, on day 3 we observed ~50% knockdown of $FOXP3^+$ Tregs in spleen (***$P <$ 0.001 by Student’s *t* test, n = 3 mice in a single animal experiment; mean ± SE; untreated: 190 ± 10 per 20× field, DT: 94 ± 24), consistent with our previously published work (13). In contrast with our prior observations in B78 melanoma tumors outside the brain, but consistent with our IHC and flow cytometry results above showing no effect of WBRT on brain tumor-infiltrating Tregs despite improved anti-tumor response, we observed no significant difference in survival among DEREG mice bearing both a flank and a brain melanoma tumor when treated with DT alone, ISV (to the flank tumor) + anti-CTLA-4, or DT + ISV + anti-CTLA-4 (Supplementary Fig. S2; https://doi.org/10.1667/RADE-20-00237.1.S1). A slight increase in survival was observed with the addition of WBRT compared to other treatment groups. Gross examination at euthanasia verified brain tumor in all mice, suggesting no confounding effect of Treg depletion on autoimmunity and subsequent mortality.

After cellular immune cell analyses using IHC and Treg depletion, molecular changes to tumor cell expression of markers of susceptibility to immune response in standard mice were tested using qRT-PCR. Increased activation of type 1 IFN response in WBRT with ISV + anti-CTLA-4 regimen was detected through increased *Mx1* gene expression, as well as increases in *Mhc-1* and *Pd-l1*, compared to untreated controls (Fig. 2B). The type 1 IFN response gene *Ifnb1* was also increased in WBRT with ISV + anti-CTLA-4 regimen but did not achieve significance (Supplementary Fig. S2; https://doi.org/10.1667/RADE-20-00237.1.S1). Previously published work by us as well as others has demonstrated that activation of a type 1 IFN response via the stimulator of interferon genes (STING) pathway by radiation is critical to enhancing anti-tumor immune response (26, 51).

Tumor-infiltrating monocytes/macrophages have been shown to be prognostic in melanoma patients treated with immunotherapies (52, 53) and radiation is known to stimulate tumor infiltration by monocyte and myeloid lineages (54–57). To begin evaluating the effect of WBRT on tumor-infiltrating monocytes/macrophages in brain melanoma tumors of mice treated with ISV + anti-CTLA-4, we performed immunohistochemistry for the monocyte/macrophage marker F4/80 on brains from mice euthanized at day 20 after treatment initiation. $F4/80^+$ cells were evident in the melanoma brain tumor for all treatment groups (Fig. 3A). Significantly increased F4/80 cell immunolabeling was observed in melanoma brain metastases for mice that received ISV + anti-CTLA-4 and WBRT + ISV + anti-CTLA-4, compared to untreated and WBRT only controls [Fig. 3B, $P < 0.05$; $n \geq 9$; mean ± SE; percentage area of 20× field labeling: Untreated: 25 ± 2.6%; WBRT (day 15, 4 Gy): 33 ± 1.9; ISV + anti-CTLA-4: 39 ± 3.1; WBRT + ISV + anti-CTLA-4: 45 ± 3.4]. We then analyzed the expression of immune-stimulatory *Nos2* and suppressive *Arg1* in the tumor microenvironment using qRT-PCR. Each was significantly upregulated in the WBRT + ISV + anti-CTLA-4 treatment group compared to the untreated and WBRT alone groups and *Arg1* was also upregulated compared to the ISV + anti-CTLA-4 treatment group (Fig. 3C). Notably, *Nos2* +expression is associated with “M1” phenotype anti-tumor macrophages/microglia while *Arg1* is associated with the “M2” immune-suppressive phenotype (14). These observations demonstrate that combining low-dose radiation with ISV + anti-CTLA-4 increases the infiltration of macrophages into a melanoma tumor in the brain and suggest that this effect may be manifest among both M1 and M2 macrophages.

Cytokine/Chemokine Profiling of Melanoma Brain Tumor after WBRT with ISV and anti-CTLA-4

Using tumor fragments from mice euthanized at day 20 after treatment initiation, we analyzed the production of cytokines and chemokines in the microenvironment of brain tumors treated with ISV + anti-CTLA-4 with or without WBRT, and controls. A multiplex cytokine immunoassay was performed, and unbiased hierarchal clustering used to sort tumors based on detected levels of cytokines/chemokines. Within melanoma brain metastases, all four treatment groups clustered, with strong distinctions observed between mice receiving WBRT and those not receiving WBRT as well as between those receiving ISV + anti-CTLA-4 and those not receiving ISV + anti-CTLA-4 (Fig. 4A). Significant changes were noted in pro-inflammatory (e.g., IFNγ, TNFα, LIX/CXCL5) and suppressive (e.g., IL10, IL13) cytokines as well as chemokines (e.g., IP-10/CXCL10, and MIG/CXCL9) (Fig. 4C). Intriguingly, despite very limited efficacy in prolonging survival or delaying intracranial tumor progression, ISV + anti-CTLA-4 resulted in potent inflammatory changes within the melanoma brain tumor microenvironment, providing evidence that the systemic immune response to this regimen was in fact propagated to the brain tumor site but was rendered ineffective in this location. In contrast, in normal brain from the contralateral striatum cytokine profiles of untreated and ISV + anti-CTLA-4-treated mice did not consistently separate in clustering analysis (Fig. 4B). This is consistent with the development of a tumor-specific response to ISV + anti-CTLA-4.

Within the brain tumor microenvironment, the expression of most cytokines/chemokines, both proinflammatory and suppressive alike, were reduced 5 days after the addition of

WBRT to ISV + anti-CTLA-4 (i.e., z-score < 0) (Fig. 4A). This contrasts with the pro-inflammatory effects that are more commonly observed after irradiation of melanoma or other tumor types in extracranial locations (58). One notable exception to this observation was CXCL5 (Fig. 4C), which was consistently upregulated in melanoma brain tumors after WBRT and extracranial delivery of ISV + anti-CTLA-4. This may suggest a critical role of CXCL5 in the metastatic melanoma brain tumor microenvironment. In addition, compared to ISV + anti-CTLA-4, the combination of WBRT + ISV + anti-CTLA-4 significantly reduced the expression of pro-inflammatory IFNγ and TNFα, chemokines IP-10/CXCL10 and MIG/CXCL9, as well as immune-suppressive IL13 in melanoma brain metastases (Fig. 4C). These observations demonstrate clear immunomodulatory effects of 4 Gy WBRT in modifying the intracranial immune response to ISV + anti-CTLA-4 and correlate with enhanced tumor control and survival with this combined treatment regimen.

A distinct pattern of chemokine/cytokine expression was also observed for samples taken from contralateral normal brain between those receiving WBRT (WBRT only, WBRT + ISV + anti-CTLA-4) and those not receiving WBRT (untreated, ISV + anti-CTLA-4) (Fig. 4B). Significant differences were observed in the concentrations of several immune-stimulatory cytokines in normal brain with addition of WBRT such as changes in pro-inflammatory IFNγ, TNFα and IL2, immune-suppressive IL10 and IL13, and chemokines IP-10/CXCL10 and MIG/CXCL9 (Fig. 4B and D). These observations illustrate the distinct effects of WBRT in the brain tumor microenvironment and the normal brain and point to the potential for toxicity to be modified by unintended immune-mediated effects of WBRT when delivered in combination with immunotherapy.

^{86}Y-NM600 Imaging/Dosimetry and ^{90}Y-NM600 Therapy to Immunomodulate Tumor in Brain

To reduce radiation effects in normal brain while still enabling immunomodulation of metastatic brain tumor microenvironments including sites that are radiographically occult and not individually targetable by external beam radiation, we tested the capacity of a targeted radionuclide therapeutic (TRT), NM600, to specifically accumulate in a melanoma tumor in the brain and deliver therapeutic radiation. NM600 is an alkylphosphocholine metal chelate which features the DOTA chelator that is selectively taken up and retained in a variety of murine and human tumor types (35, 37, 59). For imaging and dosimetry, ^{86}Yttrium (Y) was first radiochemically chelated to NM600 as described elsewhere (35, 59) and then injected into mice harboring both flank and brain melanoma (brain metastasis) tumors, verified visually or by MRI, respectively. Serial PET/CT imaging at 2, 24, 48 and 72 h after ^{86}Y-NM600 injection was then used to evaluate longitudinal uptake and retention in the brain and flank melanoma tumors. PET imaging showed specific uptake and continued retention of NM600 in melanoma (Fig. 5A and B). Increased NM600 signal was observed in melanoma brain tumors compared to normal brain at all tested time points (Fig. 5B). Tumor and normal tissue were collected at 72 h and analyzed via gamma counting. High tumor-to-normal tissue (brain for brain tumor and muscle for flank tumor) ratios were measured at both melanoma sites (Fig. 5C, n = 4, mean + SE; intracranial: 12 + 5.5; extracranial: 8.1 + 1.7). On the basis of serial ^{86}Y-NM600 PET/CT imaging, we performed Monte Carlo dosimetry calculations (35) to determine the dose of radiation delivered to brain tumor, flank tumor and normal brain as injected dose of activity per tissue mass in grams (%ID/g, Fig.

5B). Calculated total absorbed doses for melanoma tumors in brain were near 2-fold increased over normal brain and ~75% of the dose concurrently delivered to a comparable melanoma flank tumor (Fig. 5D).

In a proof-of-principle study, we tested the potential of ^{90}Y-NM600 to modify the propagation of an anti-tumor response at intracranial tumor sites when combined with an ISV + anti-CTLA-4 regimen against a flank tumor. For these experiments, mice bearing B78 melanoma brain and flank tumors were injected with an activity of ^{90}Y-NM600 that was determined from our dosimetry studies (Fig. 5A–D) to deliver 4 Gy to the melanoma brain tumor. ^{90}Y-NM600 was injected on treatment day 13 to mimic the timing of radiation delivery relative to that above with WBRT on treatment day 15, accounting for the more prolonged delivery of radiation from a TRT source. Immunohistochemical analysis of melanoma brain tumors demonstrated increases in $CD8^+$ T-cell infiltration and CD8:FOXP3 ratio with the addition of ^{90}Y-NM600 to ISV + anti-CTLA-4, with similar trends to those observed after addition of WBRT to ISV + anti-CTLA-4 (Fig. 5E). To determine whether TRT could immunomodulate a tumor microenvironment in the brain, we again analyzed cytokine levels in B78 melanoma brain tumors using a multiplex cytokine immunoassay (Fig. 5F). Cytokine profiles in melanoma brain tumors treated with TRT in combination with ISV + anti-CTLA-4 were notable for a broad reduction in the levels of nearly all evaluated peptides compared to brain tumors from ISV + anti-CTLA-4-treated mice (Fig. 5F), similar to the effects we observed at this location with the addition of WBRT to this immunotherapy regimen (Fig. 4A). When cytokine concentrations were plotted relative to ISV + anti-CTLA-4 treated mice, addition of either TRT or WBRT similarly affected IFNγ, TNFα, LIX/CXCL5, IL2, IP-10/CXCL10, MIG/CXCL9, IL10 and IL13 (Fig. 5F). Analyzing contralateral normal brain, mice receiving TRT with and without ISV + anti-CTLA-4 did not cluster closely and IFNγ was significantly reduced compared to WBRT + ISV + anti-CTLA-4 (Supplementary Fig. S3; https://doi.org/10.1667/RADE-20-00237.1.S1). Overall, these findings support our hypothesis that using TRT, as compared to WBRT, could reduce off-target immunologic effects in normal brain parenchyma, while still achieving immunomodulation of tumor microenvironments in the brain.

DISCUSSION

In this study, we tested whether the addition of low-to-moderate-dose radiation (4 Gy × 1 fraction) could potentiate the propagation of anti-tumor immunity against melanoma tumors in the brain after an ISV + anti-CTLA-4 treatment regimen in which ISV targeted a melanoma tumor outside the brain. For this, we used an immunologically “cold” B78 murine model of melanoma that does not respond to immune checkpoint blockade alone (12). Using this same tumor model, we have previously observed that our ISV + anti-CTLA-4 regimen, which effectively eliminates primary flank tumors and extracranial secondary tumors (12), has minimal efficacy against melanoma tumors in the brain (13). We report here that low-dose WBRT significantly extended survival of mice harboring intracranial melanoma when combined with ISV + anti-CTLA-4, compared to ISV + anti-CTLA-4 alone or WBRT alone.

Intriguingly, the timing of WBRT administration was critical to this therapeutic interaction. Radiation delivered to brain concurrent with flank irradiation on day 1 of the ISV + anti-

CTLA-4 regimen resulted in no additional survival benefit, whereas WBRT delivered on treatment day 15 significantly extended survival compared to ISV + anti-CTLA-4 (Fig. 1B). As WBRT on day 1 did not significantly extend survival in mice harboring intracranial melanoma, it is unlikely that cytotoxic anti-tumor effects of radiation played a major role in survival extension because these effects would be expected to have greater impact against a smaller burden of disease on treatment day 1 compared to treatment day 15. Day 15 WBRT corresponds to 5 days after completion of the ISV + anti-CTLA-4 regimen, a time at which we have previously observed the approximate peak day of T-cell response at the ISV-targeted tumor (12, 27). These survival data suggest a beneficial immune-modulatory role of 4 Gy WBRT that is not directly attributed to a cytotoxic tumor cell killing effect but rather to an immunomodulatory effect that modifies the propagation of an ISV effect against tumor sites in the brain.

In future studies it will be valuable to further explore these time-dependent effects of radiation on the propagation of anti-tumor immune response in the brain. In previously reported studies developing our ISV regimen, we similarly 006Fbserved a critical link between anti-tumor immune response and the timing of immunotherapy with a delayed interval between irradiation and immunotherapy more effective than concurrent treatment in that setting as well (12). These observations attest to the importance of temporal studies evaluating the time course of immunologic effects of radiation, as these appear to be critical to optimizing the integration of radiation therapies with immunotherapies. For example, we and others have previously reported time-dependent effects of radiation on the expression of tumor cell MHC1 and other immune-susceptibility markers and on infiltration of an irradiated tumor by Tregs (27, 51). In pilot studies, where WBRT was administered on treatment day 7 (data not shown), the effect of WBRT on survival in mice treated with ISV + anti-CTLA-4 appeared to be intermediate between that observed with WBRT on treatment day 1 and day 15. Follow-up studies may more precisely determine the optimal timing of WBRT after an extracranial ISV.

We have investigated the mechanisms whereby WBRT enhances survival in mice bearing brain melanoma tumors and treated with ISV + anti-CTLA-4. Tumor infiltration by T cells as well as monocytes/macrophages and myeloid cell lineages were quantified, and we observed an effect of ISV + anti-CTLA-4 with and without WBRT in enhancing the ratio of tumor-infiltrating $CD8^+$:$FOXP3^+$ T cells. However, no significant changes were detected when comparing WBRT + ISV + anti-CTLA-4 to the ISV + anti-CTLA-4 regimen alone. To evaluate the necessity of tumor-infiltrating Tregs to the limited response of B78 melanoma tumors in the brain to the ISV + anti-CTLA-4 regimen, we used the “DEREG” mouse model to deplete Tregs by repeated DT injections (13, 31). Surprisingly, in mice harboring intracranial melanoma, Treg depletion exhibited no survival benefit (Supplementary Fig. S2; https://doi.org/10.1667/RADE-20-00237.1.S1). This contrasts with previously published studies in extracranial murine melanoma models, which demonstrated a marked effect of Treg depletion on the propagation of anti-tumor immune response (27). Our results here suggest that Tregs are not a dominant suppressive mechanism in the B78 melanoma brain tumor model and that additional radiation-sensitive, Treg-independent suppressive factors in this melanoma brain tumor microenvironment limit propagation of ISV to intracranial sites. Overall, our evaluation of T-cell tumor infiltration in this study underscores the differences

in immunotherapeutic responses seen in intracranial and extracranial melanoma tumors and suggests that the effect of WBRT on the CD8:Treg ratio is a marker but not a driver of enhanced response at brain tumor locations.

We also quantified macrophage infiltration into melanoma brain tumors and found increases among mice treated with ISV + anti-CTLA-4 with and without WBRT (Fig. 3). The increased macrophage numbers were not surprising, as we have previously shown that ISV + anti-CTLA-4 administered to a melanoma tumor outside the brain can increase F4/80^{+} macrophages in brain metastases (13), and brain irradiation is known to recruit peripheral macrophages as well (60). However, the role these macrophages played in anti-tumor efficacy of ISV + anti-CTLA-4 and WBRT remains to be determined. PCR analyses demonstrated increased expression in the melanoma brain tumor microenvironment of both the anti-tumor M1 macrophage marker *Nos2* and the immune-suppressive M2 macrophage marker *Arg1*. Similarly, cytokines driving an “M1” phenotype such as TNFα and IFNγ were reduced with addition of WBRT to ISV + anti-CTLA-4 as well as cytokines driving an “M2” phenotype such as IL13. Therefore, it will be critical in future studies to elucidate whether and how tumor-infiltrating macrophages in this and other brain tumor models are contributing to anti-tumor immune response or to local immune suppression. These studies will be aided by new biomarkers that enable delineation of endogenous brain microglia and tumor-infiltrating macrophages as recently published studies suggest diverging roles for these related cell populations (60). In such future studies it will be valuable to also evaluate the roles of CD8 T cells and myeloid-derived suppressor cells (MDSCs) in eliciting and modulating anti-tumor immune response against tumors in the brain.

Examination of cytokines in the B78 melanoma brain tumor microenvironment revealed differences after treatment with ISV + anti-CTLA-4 with and without WBRT (Fig. 4). The single cytokine increased in the B78 brain melanoma tumor microenvironment with addition of WBRT was LIX/CXCL5. CXCL5 has been shown to exert various effects on tumor growth, microenvironment and metastases, some of which include recruitment of CD8 T cells to tumor site (61). However, in other cancers, recruitment of MDSCs by CXCL5 has mainly pro-tumor effects through inducing angiogenesis and promoting tumor cell growth (62). Further studies are now warranted to investigate the relevance of CXCL5 in the melanoma brain metastatic environment and to evaluate its effects on anti-tumor immunity in this context. Surprisingly, 30 of 32 cytokines exhibited decreased expression in the B78 melanoma brain tumor with the addition of WBRT to ISV + anti-CTLA-4. These included pro-inflammatory cytokines such as IFNγ (although not significantly different) (14, 63) and IL12, suppressive cytokines such as IL10 (64), and CD8 T-cell recruitment chemokines such as IP-10/CXCL10 and MIG/CXCL9 (62). General cytokine reduction via low-dose WBRT, when combined with ISV + anti-CTLA-4 or other immunotherapies, could affect the potential for tumor response by modifying the inflammatory response produced by immunotherapies at tumors in the brain (65–68).

Cytokine production in contralateral normal brain tissue was also altered by WBRT with and without ISV + anti-CTLA-4. Notable among these were pro-inflammatory cytokines (IFNγ and TNFα), myeloid lineage cell chemo-attractants (GM-CSF, non-significant trend towards an increase), and modifiers of immune cell activation and macrophage polarization (e.g.,

RANTES/CCL5 and MIP-1b) (14, 69–72). These results raise the possibility that immune modulation by WBRT may be mediated in part through effects in the non-tumor surrounding tissue, which could implicate resident brain cells such as reactive astrocytes and microglia (14, 63). In preclinical glioma models, radiation was used to repolarize macrophages against tumor cells resulting in increased survival (73). In this study, we have not identified which specific cells are producing specific cytokines; however, in future studies single-cell RNA sequencing or single-cell proteomic profiling could be used to clarify the source of these complex immunologic changes in the brain tissue and brain tumor microenvironment.

Our results are consistent with previously published studies showing that radiation to the whole brain, even at low doses, can induce inflammatory responses (66–68). It is possible that activation of such mechanisms in settings where immunotherapy is also being employed may modify not only tumor response but also the risks for toxicity in normal brain. We did not observe any evidence of treatment-related toxicity in this study, although further studies will be needed to evaluate potential late effects, which could occur months or years after treatment. Toxicities of WBRT have been well described in many preclinical models (74) as well as in humans clinically (25). However, the single fraction of 4 Gy WBRT delivered in this study is generally well tolerated by cancer patients and is below the threshold for many radiation-induced acute and late toxicities.

To limit the potential risk from even low-dose radiation, we tested the delivery of radiation to brain melanoma tumor sites using a TRT. The alkylphosphocholine analog, NM600, has shown tumor-specific uptake, long-term retention and therapeutic potential in a multitude of cancer types (35, 37, 59, 75). Using ^{86}Y-NM600 for PET/CT imaging, we demonstrated specific accumulation in intracranial B78 melanoma tumors with very low accumulation in normal brain (Fig. 5). Using radiotherapeutic ^{90}Y-NM600, we demonstrated that TRT can modulate T-cell infiltration and cytokine production within brain melanoma tumors (Fig. 5E and F). Interestingly, TRT in addition to ISV + anti-CTLA-4 decreased macrophages in the melanoma brain tumor environment compared to ISV + anti-CTLA-4 alone, in contrast to WBRT + ISV + anti-CTLA-4 (Figs. 3B and 5E). The effects of this difference in macrophage recruitment between TRT and WBRT will need to be elucidated in future studies. As expected from the tumor-selective delivery of radiation by NM600, cytokine production in contralateral normal brain tissue was less affected by TRT compared to WBRT (Supplementary Fig. S3; https://doi.org/10.1667/RADE-20-00237.1.S1). This is exemplified by the pro-inflammatory IFNγ, which was elevated in normal brain tissue with the addition of WBRT to ISV + anti-CTLA-4 but unaffected or slightly decreased when TRT was added to ISV + anti-CTLA-4.

We present the use of ^{90}Y-NM600 TRT for brain tumor immunomodulation here as a proof-of-concept. Additional studies will be needed to optimize this therapeutic approach. For example, the dose, half-life, range and linear energy transfer of radiation emitted from TRT sources may each impact the immune-modulatory effects of these agents. Here we demonstrate an effect of TRT on the functional immunogenicity of a tumor microenvironment through T-cell infiltration and tumor cytokine profiling. In future studies, it will be valuable to evaluate the capacity of TRT agents to augment the propagation of anti-tumor immune response at tumors in the brain and to improve survival in models and

clinical settings of brain tumors. It will be intriguing to perform comparative studies using distinct radionuclides and TRT vectors to develop a more fundamental mechanistic understanding of the interaction between TRT and the brain tumor immune microenvironment. As these approaches are tested in clinical contexts, we expect that the therapeutic window for TRT will be greater than that in mice, as the spatial distribution of dose from TRT sources to tumor and normal brain should be favorably influenced by the differences in size scale between mice and humans.

Several limitations and caveats should be noted in the current study. Only a single fraction of WBRT (4 Gy × 1) and a single dose and type of TRT were studied because our objective was to determine whether immunomodulatory effects of radiation could be observed in a brain tumor and to begin comparing effects of equal-dose WBRT and TRT in this setting. Performing dosimetry on small tumors such as these mouse brain tumors is challenging because of partial-volume effects, and uncertainty exists in dose calculations. Nevertheless, toward estimating uncertainty, injected dose per gram at 72 h calculated using PET (2.62 ± 0.77 %ID/g) agreed relatively well with *ex vivo* tissue analysis (1.94 ± 0.93 %ID/g). In addition, because of our desire to evaluate immunologic effects, these studies were performed exclusively in a syngeneic murine tumor model. Further validation of our findings in human metastatic and primary brain tumors will require clinical studies. Because the radiosensitivity of murine and human cells can vary and because cross-species variations in the immunologic effects of radiation have not been clarified for either external beam radiation or TRT, it is possible that differences will be observed between our preclinical studies in mice and future clinical studies combining TRT and immunotherapies for treatment of brain metastases. In our evaluation of the immunologic effects of radiation on the melanoma brain tumor microenvironment, we used only a single time point. This timing was selected based on our past studies in which this time point corresponded with maximal T-cell infiltration at the extracranial tumor targeted by our ISV regimen (12, 27). However, the timing of immune response at an intracranial tumor site may not directly correspond with that at a flank tumor targeted by ISV. Indeed, results described here and elsewhere (13) underscore the differences between the adaptive anti-tumor response at extracranial and brain melanoma tumors. In future studies, it will be valuable to further interrogate the time course of changes in tumor cell immune susceptibility, tumor infiltration by immune cells, and the secretion of inflammatory and suppressive cytokines/chemokines in the metastatic brain tumor microenvironment after radiation therapy.

CONCLUSIONS

Our results indicated that low-to-moderate-dose whole-brain radiation treatment or targeted radionuclide therapy can potentiate immunotherapeutic response in a melanoma tumor in the brain when combined with immune checkpoint blockade and an ISV regimen delivered to a tumor outside the brain. These data suggest possible ways to utilize low-dose radiotherapy to enhance response to immunotherapies in brain metastases and potentially for primary brain tumors. Further optimization of radiotherapeutic dose and delivery will be required, along with the investigation of additional treatment combinations, to achieve our goal of developing a treatment approach that consistently enables curative response for metastatic immunologically “cold” tumors at any location.

Supplementary Material

Refer to Web version on PubMed Central for supplementary material.

ACKNOWLEDGMENTS

We are grateful for the expert assistance provided by UWCCC Flow Cytometry, Small Animal Imaging and Radiotherapy Facility (SAIRF) and Histology/Pathology Core personnel. We also thank Apeiron Biologics, Bristol-Myers Squibb, Inc. and Archeus Technologies for providing materials used in this work. We thank the University of Wisconsin Carbone Cancer Center (UWCCC) and Small Animal Imaging and Radiotherapy Facility (SAIRF) for support of this project. This work was also supported in part by the National Institutes of Health/National Cancer Institute (NIH/NCI grant no. P30 CA014520, UW Comprehensive Cancer Center Support). This work was also supported by NIH Early Dependence Award nos. 1DP51DP5OD024576-01, U01CA233102 and P01CA250972. Funding for training was provided by UW-SMPH, and NIH awards TL1TR002375 and T32 GM008692 (JCJ) and NIH F30CA250263 (JCJ). The content of this article is solely the responsibility of the authors and does not necessarily represent the official views of the NIH. Support was also provided by generous donations from Patricia Taylor and UW Guarding Against Cancer.

REFERENCES

1. Marabelle A, Kohrt H, Caux C, Levy R. Intratumoral immunization: a new paradigm for cancer therapy. Clin Cancer Res 2014; 20:1747–56. [PubMed: 24691639]
2. Demaria S, Kawashima N, Yang AM, Devitt ML, Babb JS, Allison JP, et al. Immune-mediated inhibition of metastases after treatment with local radiation and CTLA-4 blockade in a mouse model of breast cancer. Clin Cancer Res 2005; 11:728–34. [PubMed: 15701862]
3. Rudqvist NP, Pilones KA, Lhuillier C, Wennerberg E, Sidhom JW, Emerson RO, et al. Radiotherapy and CTLA-4 blockade shape the TCR Repertoire of tumor-infiltrating T cells. Cancer Immunol Res 2018; 6:139–50. [PubMed: 29180535]
4. Sharabi AB, Nirschl CJ, Kochel CM, Nirschl TR, Francica BJ, Velarde E, et al. Stereotactic radiation therapy augments antigen-specific pd-1-mediated antitumor immune responses via cross-presentation of tumor antigen. Cancer Immunol Res 2015; 3:345–55. [PubMed: 25527358]
5. Demaria S, Ng B, Devitt ML, Babb JS, Kawashima N, Liebes L, et al. Ionizing radiation inhibition of distant untreated tumors (abscopal effect) is immune mediated. Int J Radiat Oncol Biol Phys 2004; 58:862–70. [PubMed: 14967443]
6. Dewan MZ, Galloway AE, Kawashima N, Dewyngaert JK, Babb JS, Formenti SC, et al. Fractionated but not single-dose radiotherapy induces an immune-mediated abscopal effect when combined with + anti-CTLA-4 antibody. Clin Cancer Res 2009; 15:5379–88. [PubMed: 19706802]
7. Formenti SC, Rudqvist NP, Golden E, Cooper B, Wennerberg E, Lhuillier C, et al. Radiotherapy induces responses of lung cancer to CTLA-4 blockade. Nat Med 2018; 24:1845–51. [PubMed: 30397353]
8. Twyman-Saint Victor C, Rech AJ, Maity A, Rengan R, Pauken KE, Stelekati E, et al. Radiation and dual checkpoint blockade activate non-redundant immune mechanisms in cancer. Nature 2015; 520:373–7. [PubMed: 25754329]
9. Shaverdian N, Lisberg AE, Bornazyan K, Veruttipong D, Gold-man JW, Formenti SC, et al. Previous radiotherapy and the clinical activity and toxicity of pembrolizumab in the treatment of non-small-cell lung cancer: a secondary analysis of the KEYNOTE-001 phase 1 trial. Lancet Oncol 2017; 18:895–903. [PubMed: 28551359]
10. Theelen W, Lalezari F, de Vries J, De Langen J, Aerts J, Monkhorst K, et al. Randomized phase II study of pembrolizumab after stereotactic body radiotherapy (SBRT) versus pembrolizumab alone in patients with advanced non-small cell lung cancer: The PEMBRO-RT study. J Clin Oncol 2018; 36:Abstract 9023.
11. McBride SM, Sherman EJ, Tsai CJ, Baxi SS, Aghalar J, Eng J, et al. A phase II randomized trial of nivolumab with stereotactic body radiotherapy (SBRT) versus nivolumab alone in metastatic (M1) head and neck squamous cell carcinoma (HNSCC). J Clin Oncol 2018; 36:6009.

12. Morris ZS, Guy EI, Francis DM, Gressett MM, Werner LR, Carmichael LL, et al. In situ tumor vaccination by combining local radiation and tumor-specific antibody or immunocytokine treatments. Cancer Res 2016; 76:3929–41. [PubMed: 27197149]
13. Clark PA, Sriramaneni RN, Jin WJ, Jagodinsky JC, Bates AM, Jaquish AA, et al. In situ vaccination at a peripheral tumor site augments response against melanoma brain metastases. J Immunother Cancer 2020; 8: e000809. [PubMed: 32690669]
14. Ransohoff RM, Brown MA. Innate immunity in the central nervous system. J Clin Invest 2012; 122:1164–71. [PubMed: 22466658]
15. Wakim LM, Woodward-Davis A, Liu R, Hu Y, Villadangos J, Smyth G, et al. The molecular signature of tissue resident memory CD8 T cells isolated from the brain. J Immunol 2012; 189, 3462–71. [PubMed: 22922816]
16. Kipnis J, Multifaceted interactions between adaptive immunity and the central nervous system. Science 2016; 353, 766–71. [PubMed: 27540163]
17. Benbenishty A, Gadrich M, Cottarelli A, Lubart A, Kain D, Amer M, et al. Prophylactic TLR9 stimulation reduces brain metastasis through microglia activation. PLoS Biol 2019; 17:e2006859. [PubMed: 30921319]
18. Priego N, Zhu L, Monteiro C, Mulders M, Wasilewski D, Bindeman W, et al. STAT3 labels a subpopulation of reactive astrocytes required for brain metastasis. Nat Med 2018; 24:1024–35. [PubMed: 29892069]
19. Schwartz H, Blacher E, Amer M, Livneh N, Abramovitz L, Klein A, et al. Incipient melanoma brain metastases instigate astrogliosis and neuroinflammation. Cancer Res 2016; 76:4359–71. [PubMed: 27261506]
20. Achrol AS, Rennert RC, Anders C, Soffietti R, Ahluwalia MS, Nayak L, et al. Brain metastases. Nat Rev Dis Primers 2019; 5:5. [PubMed: 30655533]
21. Schadendorf D, van Akkooi ACJ, Berking C, Griewank KG, Gutzmer R, Hauschild A, et al. Melanoma. Lancet 2018; 392:971–84. [PubMed: 30238891]
22. Parakh S, Park JJ, Mendis S, Rai R, Xu W, Lo S, et al. Efficacy of anti-PD-1 therapy in patients with melanoma brain metastases. Br J Cancer 2017; 116:1558–63. [PubMed: 28524161]
23. Long GV, Atkinson V, Lo S, Sandhu S, Guminski AD, Brown MP, et al. Combination nivolumab and ipilimumab or nivolumab alone in melanoma brain metastases: a multicentre randomised phase 2 study. Lancet Oncol 2018; 19:672–81. [PubMed: 29602646]
24. Tawbi HA, Forsyth PA, Algazi A, Hamid O, Hodi FS, Moschos SJ, et al. Combined nivolumab and ipilimumab in melanoma metastatic to the brain. N Engl J Med 2018; 379:722–30. [PubMed: 30134131]
25. Aizer AA, Lee EQ. Brain metastases. Neurol Clin 2018; 36:557–77. [PubMed: 30072071]
26. Vanpouille-Box C, Alard A, Aryankalayil MJ, Sarfraz Y, Diamond JM, Schneider RJ, et al. DNA exonuclease Trex1 regulates radiotherapy-induced tumour immunogenicity. Nat Commun 2017; 8:15618. [PubMed: 28598415]
27. Morris ZS, Guy EI, Werner LR, Carlson PM, Heinze CM, Kler JS, et al. Tumor-specific inhibition of in situ vaccination by distant untreated tumor sites. Cancer Immunol Res 2018; 6:825–34. [PubMed: 29748391]
28. Newcomb EW, Demaria S, Lukyanov Y, Shao Y, Schnee T, Kawashima N, et al. The combination of ionizing radiation and peripheral vaccination produces long-term survival of mice bearing established invasive GL261 gliomas. Clin Cancer Res 2006; 12:4730–7. [PubMed: 16899624]
29. Haraguchi M, Yamashiro S, Yamamoto A, Furukawa K, Takamiya K, Lloyd KO, et al. Isolation of GD3 synthase gene by expression cloning of GM3 alpha-2,8-sialyltransferase cDNA using anti-GD2 monoclonal antibody. Proc Natl Acad Sci U S A 1994; 91:10455–9. [PubMed: 7937974]
30. Lahl K, Sparwasser T. In vivo depletion of FoxP3+ Tregs using the DEREG mouse model. Methods Mol Biol 2011; 707:157–72. [PubMed: 21287334]
31. Lahl K, Loddenkemper C, Drouin C, Freyer J, Arnason J, Eberl G, et al. Selective depletion of Foxp3+ regulatory T cells induces a scurfy-like disease. J Exp Med 2007; 204:57–63. [PubMed: 17200412]

32. Gillies SD, Reilly EB, Lo KM, Reisfeld RA. Antibody-targeted interleukin 2 stimulates T-cell killing of autologous tumor cells. Proc Natl Acad Sci U S A 1992; 89:1428–32. [PubMed: 1741398]
33. Zhang S, Cordon-Cardo C, Zhang HS, Reuter VE, Adluri S, Hamilton WB, et al. Selection of tumor antigens as targets for immune attack using immunohistochemistry: I. Focus on gangliosides. Int J Cancer 1997; 73:42–9. [PubMed: 9334808]
34. Aluicio-Sarduy E, Hernandez R, Valdovinos HF, Kutyreff CJ, Ellison PA, Barnhart TE, et al. Simplified and automatable radiochemical separation strategy for the production of radiopharmaceutical quality (86)Y using single column extraction chromatography. Appl Radiat Isot 2018; 142:28–31. [PubMed: 30245439]
35. Grudzinski JJ, Hernandez R, Marsh I, Patel RB, Aluicio-Sarduy E, Engle J, et al. Preclinical characterization of 86/90Y-NM600 in a variety of murine and human cancer tumor models. J Nucl Med 2019; 60:1622–8. [PubMed: 30954941]
36. Clark PA, Iida M, Treisman DM, Kalluri H, Ezhilan S, Zorniak M, et al. Activation of multiple ERBB family receptors mediates glioblastoma cancer stem-like cell resistance to EGFR-targeted inhibition. Neoplasia 2012; 14:420–8. [PubMed: 22745588]
37. Hernandez R, Walker KL, Grudzinski JJ, Aluicio-Sarduy E, Patel R, Zahm CD, et al. Y-NM600 targeted radionuclide therapy induces immunologic memory in syngeneic models of T-cell non-Hodgkin's Lymphoma. Commun Biol 2019; 2:79. [PubMed: 30820474]
38. Bednarz B, Grudzinski J, Marsh I, Besemer A, Baiu D, Weichert J, et al. Murine-specific internal dosimetry for preclinical investigations of imaging and therapeutic agents. Health Phys 2018; 114:450–59. [PubMed: 29481536]
39. Marsh IR, Grudzinski J, Baiu DC, Besemer A, Hernandez R, Jeffery JJ, et al. Preclinical pharmacokinetics and dosimetry studies of 124I/131I-CLR1404 for treatment of pediatric solid tumors in murine xenograft models. J Nucl Med 2019; 60:1414–20. [PubMed: 30926646]
40. Besemer AE, Hall LT, Bednarz BP. In-human validation of the use of pre-treatment molecular imaging for the prediction of patient-specific dosimetry in targeted radionuclide therapy (TRT). Mol Imaging Biol 2016; 18, S1570–1.
41. Besemer AE, Yang YM, Grudzinski JJ, Hall LT, Bednarz BP. Development and validation of RAPID: A patient-specific Monte Carlo three-dimensional internal dosimetry platform. Cancer Biother Radiopharm 2018; 33:155–65. [PubMed: 29694246]
42. Besemer AE, Titz B, Grudzinski JJ, Weichert JP, Kuo JS, Robins HI, et al. Impact of PET and MRI threshold-based tumor volume segmentation on patient-specific targeted radionuclide therapy dosimetry using CLR1404. Phys Med Biol 2017; 62:6008–25. [PubMed: 28682793]
43. Yang RK, Kalogriopoulos NA, Rakhmilevich AL, Ranheim EA, Seo S, Kim K, et al. Intratumoral hu14.18-IL-2 (IC) induces local and systemic antitumor effects that involve both activated T and NK cells as well as enhanced IC retention. J Immunol 2012; 189:2656–64. [PubMed: 22844125]
44. Alderson KL, Luangrath M, Elsenheimer MM, Gillies SD, Navid F, Rakhmilevich AL, et al. Enhancement of the anti-melanoma response of Hu14.18K322A by αCD40 + CpG. Cancer Immunol Immunother 2013; 62:665–75. [PubMed: 23151945]
45. Maecker HT, Trotter J. Flow cytometry controls, instrument setup, and the determination of positivity. Cytometry A 2006; 69:1037–42. [PubMed: 16888771]
46. Broom BM, Ryan MC, Brown RE, Ikeda F, Stucky M, Kane DW, et al. A galaxy implementation of next-generation clustered heatmaps for interactive exploration of molecular profiling data. Cancer Res 2017; 77:e23–6. [PubMed: 29092932]
47. Ullman-Cullere MH, Foltz CJ. Body condition scoring: a rapid and accurate method for assessing health status in mice. Lab Anim Sci 1999; 49:319–23. [PubMed: 10403450]
48. Quezada SA, Peggs KS, Curran MA, Allison JP. CTLA4 blockade and GM-CSF combination immunotherapy alters the intratumor balance of effector and regulatory T cells. J Clin Invest 2006; 116:1935–45. [PubMed: 16778987]
49. Jacobs JF, Nierkens S, Figdor CG, de Vries IJ, Adema GJ. Regulatory T cells in melanoma: the final hurdle towards effective immunotherapy? Lancet Oncol 2012; 13:e32–42. [PubMed: 22225723]

50. Curran MA, Montalvo W, Yagita H, Allison JP. PD-1 and CTLA-4 combination blockade expands infiltrating T cells and reduces regulatory T and myeloid cells within B16 melanoma tumors. Proc Natl Acad Sci U S A 2010; 107:4275–80. [PubMed: 20160101]
51. Werner LR, Kler JS, Gressett MM, Riegert M, Werner LK, Heinze CM, et al. Transcriptional-mediated effects of radiation on the expression of immune susceptibility markers in melanoma. Radiother Oncol 2017; 124:418–26. [PubMed: 28893414]
52. Melief SM, Visconti VV, Visser M, van Diepen M, Kapiteijn EH, van den Berg JH, et al. Long-term survival and clinical benefit from adoptive T-cell transfer in stage IV melanoma patients is determined by a four-parameter tumor immune signature. Cancer Immunol Res 2017; 5:170–9. [PubMed: 28073773]
53. Gartrell RD, Marks DK, Hart TD, Li G, Davari DR, Wu A, et al. Quantitative analysis of immune infiltrates in primary melanoma. Cancer Immunol Res 2018; 6:481–93. [PubMed: 29467127]
54. Vatner RE, Formenti SC. Myeloid-derived cells in tumors: effects of radiation. Semin Radiat Oncol 2015; 25:18–27. [PubMed: 25481262]
55. Kim S, Choe JH, Lee GJ, Kim YS, Kim SY, Lee HM, et al. Ionizing radiation induces innate immune responses in macrophages by generation of mitochondrial reactive oxygen species. Radiat Res 2017; 187:32–41. [PubMed: 28001907]
56. Teresa Pinto A, Laranjeiro Pinto M, Patricia Cardoso A, Monteiro C, Teixeira Pinto M, Filipe Maia A, et al. Ionizing radiation modulates human macrophages towards a pro-inflammatory phenotype preserving their pro-invasive and pro-angiogenic capacities. Sci Rep 2016; 6:18765. [PubMed: 26735768]
57. Leblond MM, Peres EA, Helaine C, Gerault AN, Moulin D, Anfray C, et al. M2 macrophages are more resistant than M1 macrophages following radiation therapy in the context of glioblastoma. Oncotarget 2017; 8:72597–612. [PubMed: 29069812]
58. Di Maggio FM, Minafra L, Forte GI, Cammarata FP, Lio D, Messa C, et al. Portrait of inflammatory response to ionizing radiation treatment. J Inflamm (Lond) 2015; 12:14. [PubMed: 25705130]
59. Hernandez R, Grudzinski JJ, Aluicio-Sarduy E, Massey CF, Pinchuk AN, Bitton AN, et al. (177)Lu-NM600 targeted radionuclide therapy extends survival in syngeneic murine models of triple-negative breast cancer. J Nucl Med 2020; 61:1187–94. [PubMed: 31862799]
60. Sevenich L. Turning “cold” into “hot” tumors–opportunities and challenges for radio-immunotherapy against primary and metastatic brain cancers. Front Oncol 2019; 9:163. [PubMed: 30941312]
61. Zhang W, Wang H, Sun M, Deng X, Wu X, Ma Y, et al. CXCL5/CXCR2 axis in tumor microenvironment as potential diagnostic biomarker and therapeutic target. Cancer Commun (Lond) 2020; 40:69–80. [PubMed: 32237072]
62. Nagarsheth N, Wicha MS, Zou W. Chemokines in the cancer microenvironment and their relevance in cancer immunotherapy. Nat Rev Immunol 2017; 17:559–72. [PubMed: 28555670]
63. Quail DF, Joyce JA. The microenvironmental landscape of brain tumors. Cancer Cell 2017; 31:326–41. [PubMed: 28292436]
64. Ouyang W, O’Garra A. IL-10 family cytokines IL-10 and IL-22: from basic science to clinical translation. Immunity 2019; 50:871–91. [PubMed: 30995504]
65. Perrinjaquet C, Desbaillets N, Hottinger AF. Neurotoxicity associated with cancer immunotherapy: immune checkpoint inhibitors and chimeric antigen receptor T-cell therapy. Curr Opin Neurol 2019; 32:500–10. [PubMed: 30893101]
66. Schaue D, Kachikwu EL, McBride WH. Cytokines in radiobiological responses: a review. Radiat Res 2012; 178:505–23. [PubMed: 23106210]
67. Lumniczky K, Szatmari T, Safrany G. Ionizing radiation-induced immune and inflammatory reactions in the brain. Front Immunol 2017; 8:517. [PubMed: 28529513]
68. Schroder S, Kriesen S, Paape D, Hildebrandt G, Manda K. Modulation of inflammatory reactions by low-dose ionizing radiation: Cytokine release of murine endothelial cells is dependent on culture conditions. J Immunol Res 2018; 2018:2856518. [PubMed: 29967799]
69. Engelhardt B, Ransohoff RM. Capture, crawl, cross: the T cell code to breach the blood-brain barriers. Trends Immunol 2012; 33:579–89. [PubMed: 22926201]

70. Becher B, Bechmann I, Greter M. Antigen presentation in autoimmunity and CNS inflammation: how T lymphocytes recognize the brain. J Mol Med (Berl) 2006; 84:532–43. [PubMed: 16773356]

71. Cherry JD, Olschowka JA, O'Banion MK. Neuroinflammation and M2 microglia: the good, the bad, and the inflamed. J Neuroinflammation 2014; 11:98. [PubMed: 24889886]

72. Dangaj D, Bruand M, Grimm AJ, Ronet C, Barras D, Duttagupta PA, et al. Cooperation between constitutive and inducible chemokines enables T cell engraftment and immune attack in solid tumors. Cancer Cell 2019; 35:885–900.e10. [PubMed: 31185212]

73. Stessin AM, Clausi MG, Zhao Z, Lin H, Hou W, Jiang Z, et al. Repolarized macrophages, induced by intermediate stereotactic dose radiotherapy and immune checkpoint blockade, contribute to long-term survival in glioma-bearing mice. J Neurooncol 2020; 147:547–55. [PubMed: 32215786]

74. Yang L, Yang J, Li G, Li Y, Wu R, Cheng J, et al. Pathophysiological responses in rat and mouse models of radiation-induced brain injury. Mol Neurobiol 2017; 54:1022–32. [PubMed: 26797684]

75. Weichert JP, Clark PA, Kandela IK, Vaccaro AM, Clarke W, Longino MA, et al. Alkylphosphocholine analogs for broad-spectrum cancer imaging and therapy. Sci Transl Med 2014; 6:240ra75.

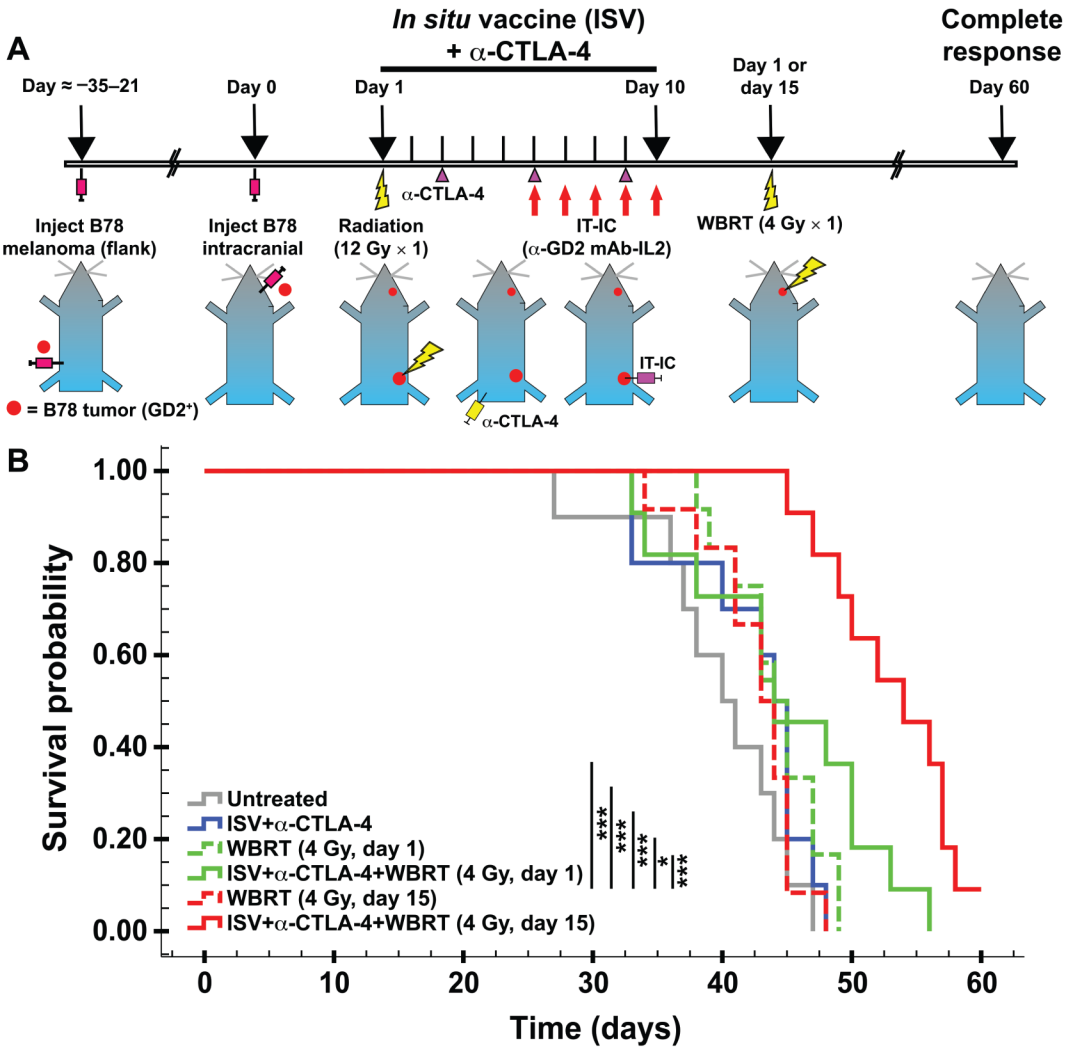

FIG. 1.

Panel A: Experimental timeline for addition of low-to-moderate-dose whole-brain radiation treatment (WBRT) to *in situ* vaccination (ISV) + anti-CTLA-4 (a-CTLA-4) regimen. The ISV approach includes radiation and IT-IC. Panel B: Survival curve for mice receiving WBRT in addition to ISV + anti-CTLA-4 regimen, and treatment controls (**$P < 0.01$, ***$P < 0.001$, Kaplan-Meier, n ≥ 10, at least two independent animal experiments).

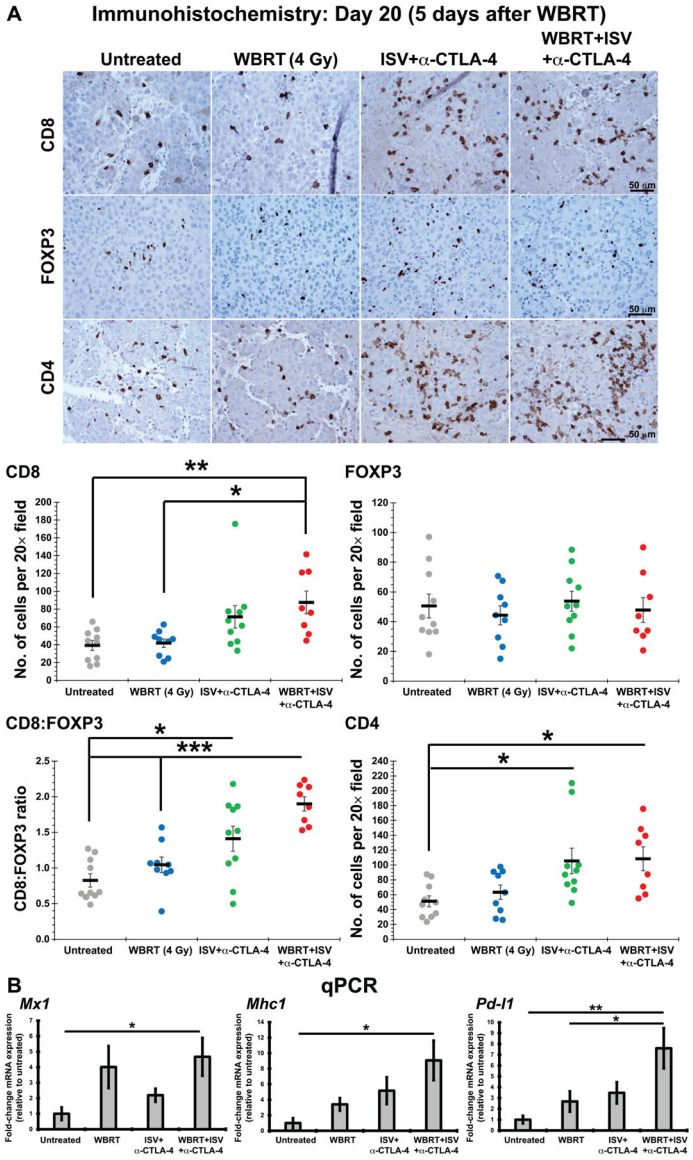

FIG. 2.

Panel A: Immunohistochemistry for T-cell markers 5 days after WBRT [4 Gy × 1, administered on day 20 of *in situ* vaccine (ISV) + anti-CTLA-4 (a-CTLA-4) regimen] compared to those of untreated and single-treatment controls (brown = positive immunolabeling), and quantified [$***P < 0.001$, $**P < 0.01$, $*P < 0.05$, mean ± SE with marker representing each individual mouse (i.e., average of 3 high-powered fields), ANOVA with post hoc Bonferroni, n ≥ 9 in at least 2 independent animal experiments]. Panel B: qRT-PCR analysis for expression of tumor immune-susceptibility genes *Mx1*, *Mhc1* and *Pd-l1* in melanoma brain tumors of standard mice at 5 days after WBRT + ISV + anti-CTLA-4, compared to those of single-treatment and untreated controls ($**P < 0.01$, $*P < 0.05$, shown as fold-change increase from untreated controls, mean ± SE, ANOVA with post hoc Bonferroni, n ≥ 8 in at least two independent animal experiments).

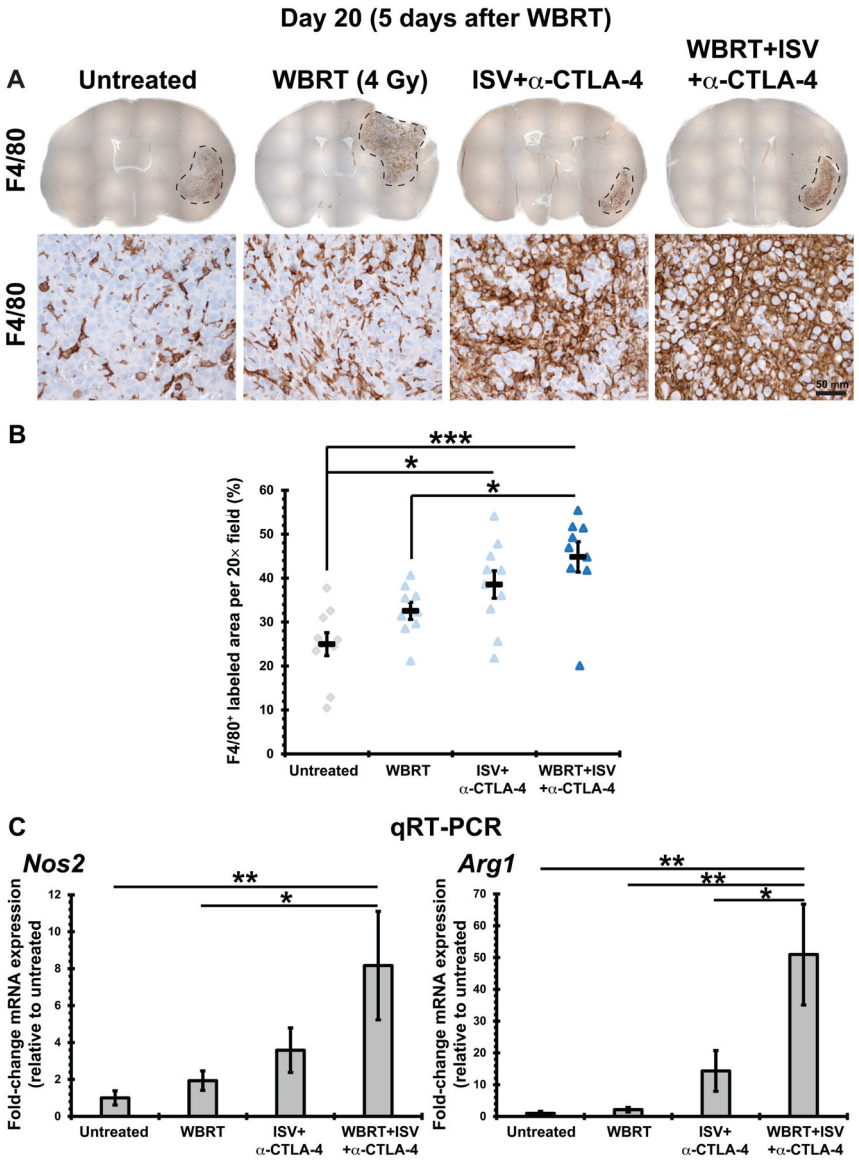

FIG. 3.

Panel A: Whole brain and photomicrographs for monocyte/macrophage marker F4/80 at 5 days after WBRT (4 Gy × 1, administered on day 20 of ISV + anti-CTLA-4 regimen) compared to untreated and single-treatment controls (dotted line = tumor area determined by serial H&E slides; brown = positive immunolabeling), and (panel B) quantified [***$P <$ 0.001, *$P <$ 0.05, mean ± SE with marker representing each individual mouse (i.e., average of 3 high-powered fields), ANOVA with post hoc Bonferroni, n ≥ 9, at least two independent animal experiments]. Panel C: qRT-PCR analysis for expression of immune-stimulatory *Nos2* and -suppressive *Arg1* in melanoma brain tumors at 5 days after WBRT + ISV + anti-CTLA-4, compared to single-treatment and untreated controls (**$P <$ 0.01, *$P <$ 0.05, shown as fold-change increase from untreated controls, mean ± SE, ANOVA with post hoc Bonferroni, n ≥ 8 in at least two independent animal experiments).

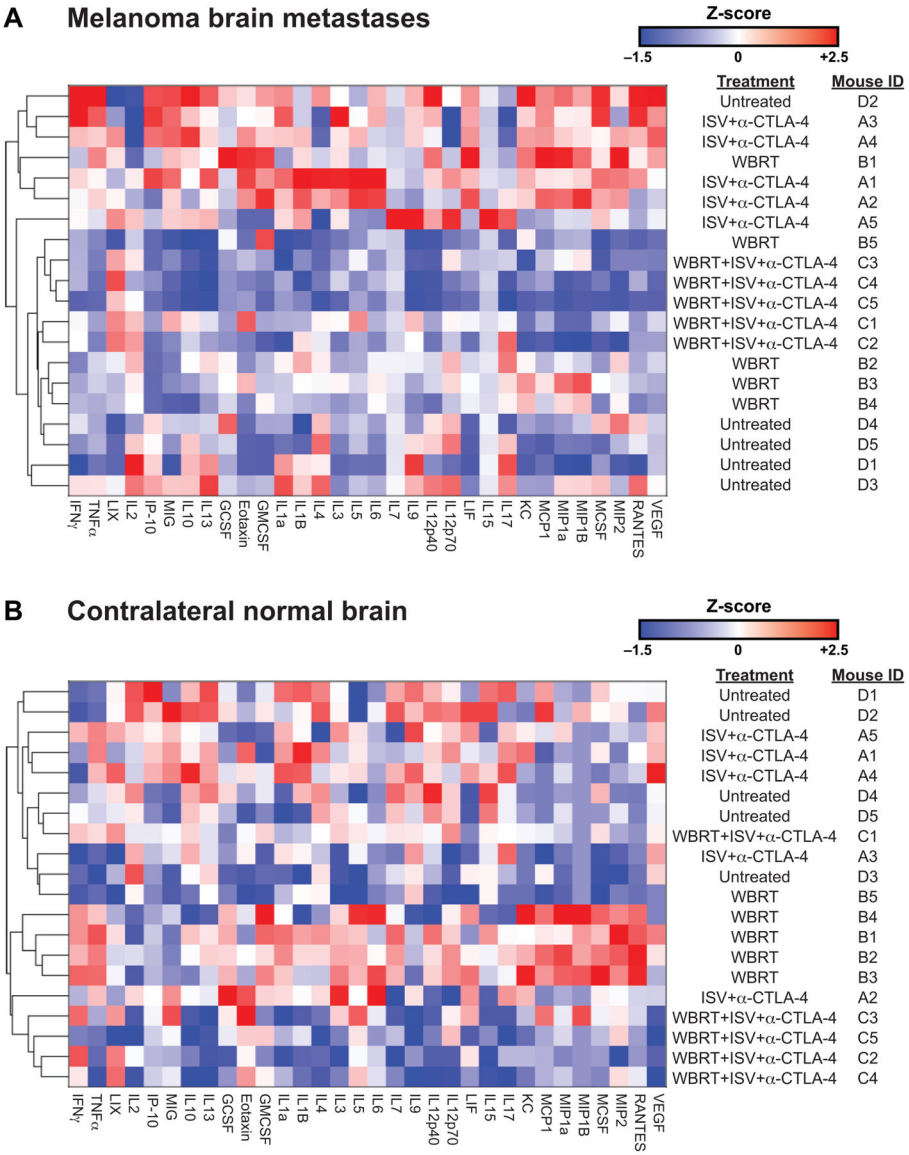

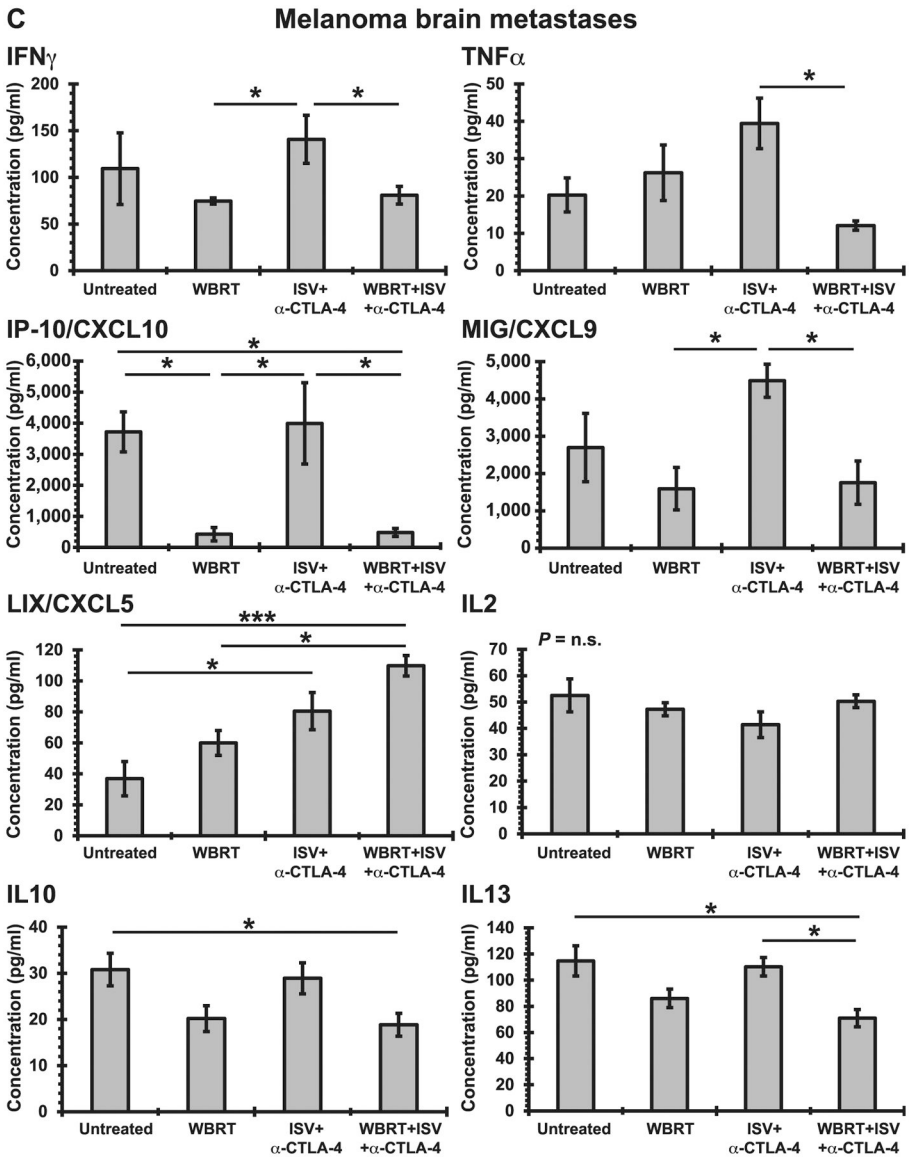

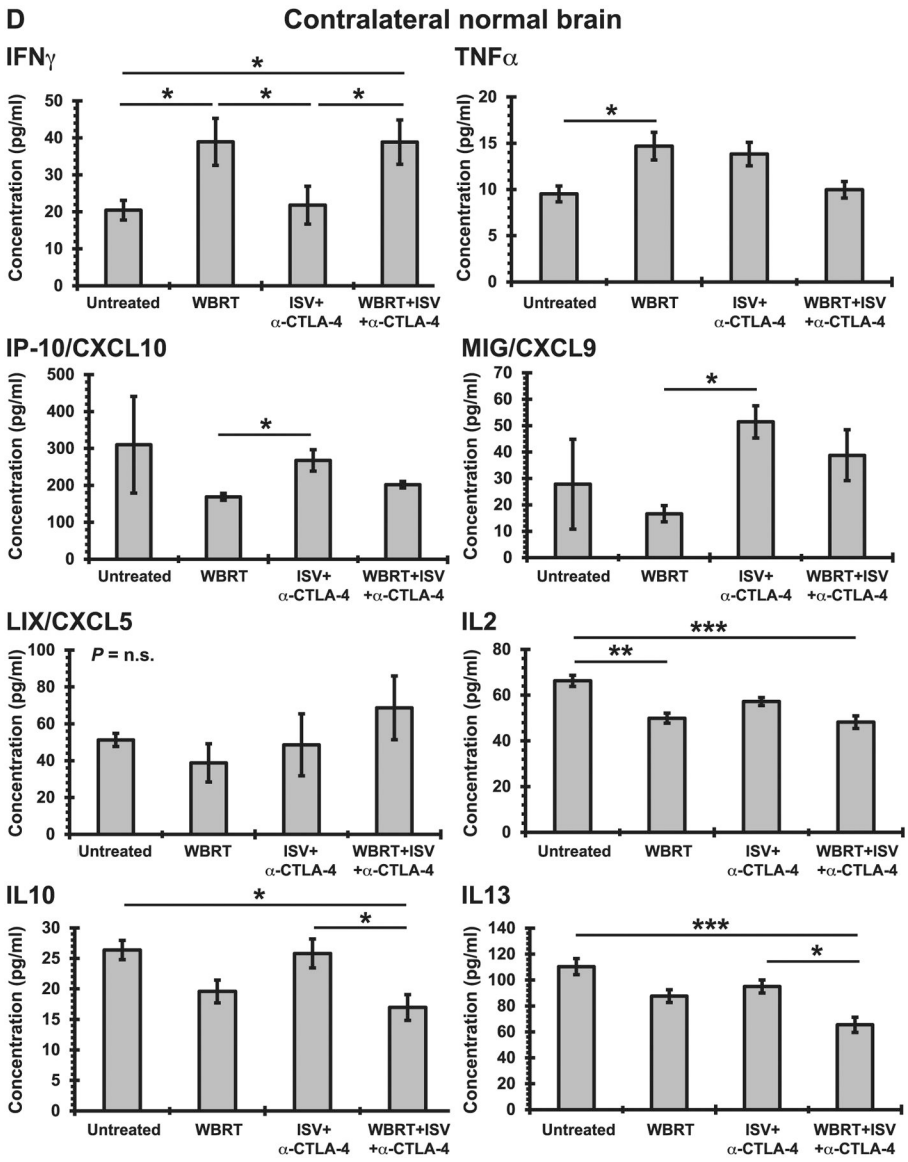

FIG. 4.

Panel A: Heatmap of cytokines/chemokines analyzed via multiplex immunoassay hierarchically clustered by treatment for both melanoma brain tumors and contralateral normal brain, respectively, in mice that received WBRT + ISV + anti-CTLA-4 regimen and treatment controls (z-scores; n = 5 mice in a single animal experiment). Panels C and D: Concentrations of individual cytokines/chemokines for both melanoma brain tumors and contralateral normal brain, respectively, in mice receiving WBRT ISV + anti-CTLA-4 regimen and treatment controls (***$P < 0.001$, **$P < 0.01$, *$P < 0.05$, mean ± SE, ANOVA with post hoc Bonferroni, n=5 in a single animal experiment).

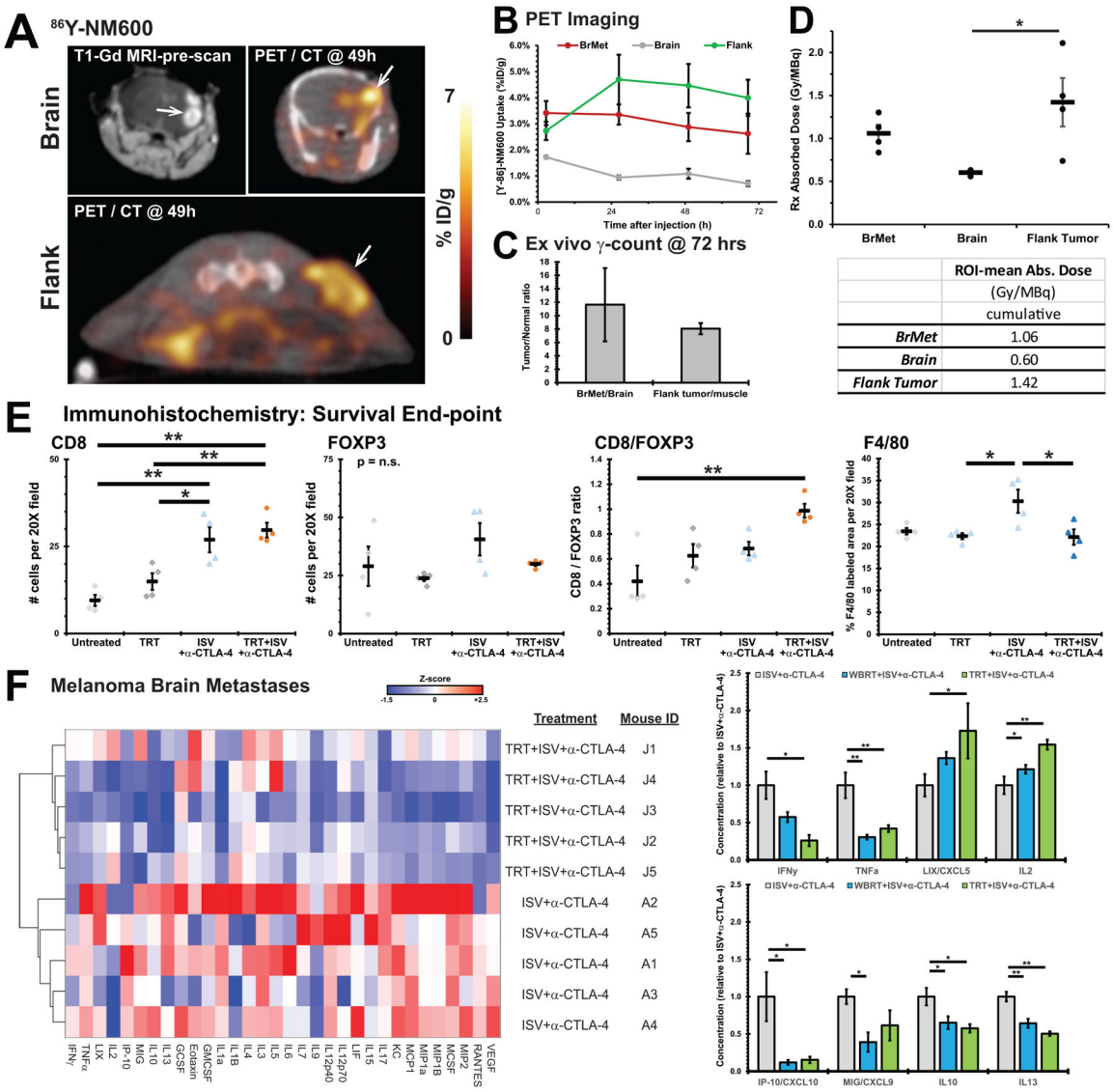

FIG. 5.

Panel A: MRI (T1 with gadolinium contrast) was used to verify presence of melanoma brain metastasis (arrow). ^{86}Y-NM600 was then injected and imaged longitudinally using PET/CT imaging, and at 49 h after injection, demonstrated selective uptake into both brain metastasis and flank melanoma tumors (%ID/g = percentage injected dose per gram; arrow indicates tumor; secondary signal in flank is likely hepatobiliary/fecal). Panel B: ^{86}Y-NM600 uptake and retention up to 72 h demonstrated increased drug uptake in melanoma brain metastasis and flank tumors compared to normal brain (mean ± SE, n = 4 in a single animal experiment). Panel C: *Ex vivo* gamma counts of tissue at 72 h showed similar tumor/normal ratios comparing melanoma brain metastasis to flank tumors (mean ± SE, n = 4 in a single animal experiment). Panel D: Monte Carlo dosimetry calculations were performed to determine the dose of radiation (Gy/MBq) delivered to melanoma brain metastasis and flank tumor, and normal brain (mean ± SE, with each dot representing an individual mouse, $*P <$ 0.05, ANOVA with post hoc Bonferroni, n = 4 in a single animal experiment). Panel E:

Quantified immunohistochemistry for T-cell markers after administration of targeted radionuclide therapy (TRT) ^{90}Y-NM600 with and without ISV + anti-CTLA-4 regimen, with samples taken at euthanasia for survival end point and compared to untreated controls [$^{**}P < 0.01$, $^{*}P < 0.05$, mean ± SE with marker representing each individual mouse (i.e., average of 3 high-powered fields), ANOVA with post hoc Bonferroni, n = 4 in a single animal experiment]. Panel F: Heatmap of cytokines/chemokines analyzed via multiplex immunoassay for melanoma brain metastases in mice treated with TRT ^{90}Y-NM600 with and without ISV+ anti-CTLA-4 regimen (z-scores; n = 5 mice in a single animal experiment). Concentrations of cytokines/chemokines in mice treated with TRT ^{90}Y-NM600 or WBRT with ISV+ anti-CTLA-4 regimen, plotted relative to ISV + anti-CTLA-4 regimen alone ($^{**}P < 0.01$, $^{*}P < 0.05$, mean ± SE, ANOVA with post hoc Bonferroni, n = 5 in a single animal experiment).